Atmos. Chem. Phys., 16, 4785–4797, 2016
www.atmos-chem-phys.net/16/4785/2016/
doi:10.5194/acp-16-4785-2016

Atmospheric Chemistry and Physics Open Access EGU

Introduction: Observations and Modeling of the Green Ocean Amazon (GoAmazon2014/5)

S. T. Martin[1], P. Artaxo[2], L. A. T. Machado[3], A. O. Manzi[4], R. A. F. Souza[5], C. Schumacher[6], J. Wang[7], M. O. Andreae[8], H. M. J. Barbosa[2], J. Fan[9], G. Fisch[10], A. H. Goldstein[11], A. Guenther[12], J. L. Jimenez[13], U. Pöschl[8], M. A. Silva Dias[2], J. N. Smith[12], and M. Wendisch[14]

[1]Harvard University, Cambridge, Massachusetts, USA
[2]University of São Paulo, São Paulo, Brazil
[3]National Institute for Space Research, São José dos Campos, Brazil
[4]National Institute of Amazonian Research, Manaus, Amazonas, Brazil
[5]Amazonas State University, Amazonas, Brazil
[6]Texas A&M University, College Station, Texas, USA
[7]Brookhaven National Laboratory, Upton, New York, USA
[8]Max Planck Institute for Chemistry, Departments of Biogeochemistry and Multiphase Chemistry, Mainz, Germany
[9]Pacific Northwest National Laboratory, Richland, Washington, USA
[10]Aeronautic and Space Institute, São José dos Campos, Brazil
[11]University of California, Berkeley, California, USA
[12]University of California, Irvine, California, USA
[13]University of Colorado, Boulder, Colorado, USA
[14]University of Leipzig, Leipzig, Germany

Correspondence to: S. T. Martin (scot_martin@harvard.edu)

Received: 2 October 2015 – Published in Atmos. Chem. Phys. Discuss.: 4 November 2015
Revised: 10 March 2016 – Accepted: 5 April 2016 – Published: 19 April 2016

Abstract. The Observations and Modeling of the Green Ocean Amazon (GoAmazon2014/5) Experiment was carried out in the environs of Manaus, Brazil, in the central region of the Amazon basin for 2 years from 1 January 2014 through 31 December 2015. The experiment focused on the complex interactions among vegetation, atmospheric chemistry, and aerosol production on the one hand and their connections to aerosols, clouds, and precipitation on the other. The objective was to understand and quantify these linked processes, first under natural conditions to obtain a baseline and second when altered by the effects of human activities. To this end, the pollution plume from the Manaus metropolis, superimposed on the background conditions of the central Amazon basin, served as a natural laboratory. The present paper, as the introduction to the special issue of GoAmazon2014/5, presents the context and motivation of the GoAmazon2014/5 Experiment. The nine research sites, including the characteristics and instrumentation of each site, are presented. The sites range from time point zero (T0) upwind of the pollution, to T1 in the midst of the pollution, to T2 just downwind of the pollution, to T3 furthest downwind of the pollution (70 km). In addition to the ground sites, a low-altitude G-159 Gulfstream I (G-1) observed the atmospheric boundary layer and low clouds, and a high-altitude Gulfstream G550 (HALO) operated in the free troposphere. During the 2-year experiment, two Intensive Operating Periods (IOP1 and IOP2) also took place that included additional specialized research instrumentation at the ground sites as well as flights of the two aircraft. GoAmazon2014/5 IOP1 was carried out from 1 February to 31 March 2014 in the wet season. GoAmazon2014/5 IOP2 was conducted from 15 August to 15 October 2014 in the dry season. The G-1 aircraft flew during both IOP1 and IOP2, and the HALO aircraft flew during IOP2. In the context of the Amazon basin, the two IOPs also correspond to the clean and biomass burning seasons, respectively. The Manaus plume is

present year-round, and it is transported by prevailing northeasterly and easterly winds in the wet and dry seasons, respectively. This introduction also organizes information relevant to many papers in the special issue. Information is provided on the vehicle fleet, power plants, and industrial activities of Manaus. The mesoscale and synoptic meteorologies relevant to the two IOPs are presented. Regional and long-range transport of emissions during the two IOPs is discussed based on satellite observations across South America and Africa. Fire locations throughout the airshed are detailed. In conjunction with the context and motivation of GoAmazon2014/5 as presented in this introduction, research articles including thematic overview articles are anticipated in this special issue to describe the detailed results and findings of the GoAmazon2014/5 Experiment.

1 Introduction

The Amazon basin functions as a giant biogeochemical reactor to influence regional climate, with both exports and imports of climate-relevant quantities to and from other regions of Earth (Keller et al., 2009). Biogenic emissions of gases and aerosol particles, in combination with high absolute humidity and strong solar radiation, maintain chemical and physical cycles that sustain the aerosol particle population, the cloud field, and the hydrological cycle of the basin (Salati and Vose, 1984; Lelieveld et al., 2008; Martin et al., 2010a). The biology of the forest has a critical role in regulating atmospheric composition and climate over the region (Pöschl et al., 2010; Artaxo et al., 2013).

Any accurate model of the Earth system must succeed in a good description of tropical regions and in particular the Amazon basin, both in its natural state as well as when perturbed by regional and global human activities. The hydrologic cycle of the basin is one of the primary heat engines of global circulation (Nobre et al., 2009). Models of future climate accounting for human activities have suggested a possible drying, especially in the eastern regions (Nobre et al., 1991; Boisier et al., 2015). Significant changes in the amounts and patterns of precipitation in the basin can have far-reaching consequences because of the nonlinear, multiscale interactions that affect clouds, precipitation, and atmospheric circulation, leading for example to possible modifications in the annual migration of the Intertropical Convergence Zone (ITCZ) (Wang and Fu, 2007). The hydrological cycle in the Amazon basin has changed over the past 2 decades, but the causes are not fully identified and understood (Davidson et al., 2012; Gloor et al., 2013).

At present, many aspects of continental tropical deep convection, such as the daily cycle, are poorly understood and inaccurately modeled (Betts, 2002; Dai, 2006). Cloud properties simulated in climate models have high sensitivity to changes in droplet concentration, droplet size distribution, and liquid water content (Dandin et al., 1997; Liu and Daum, 2002; Rotstayn and Liu, 2003). Cloud microphysical properties, cloud cover, precipitation, lightning, and regional climate over the Amazon basin can be significantly affected by aerosol particles (Andreae et al., 2004; Lin et al., 2006; Rosenfeld et al., 2008, 2014; Martins and Silva Dias, 2009; Altaratz et al., 2010; Koren et al., 2012; Gonçalves et al., 2015). For background conditions in the basin, aerosol particle concentrations at Earth's surface number several hundred per cubic centimeter in the wet season (Andreae, 2007; Martin et al., 2010a). By comparison, background concentrations increase by an order of magnitude in the dry season because of widespread biomass burning (Martin et al., 2010a; Artaxo et al., 2013). Shifts in the concentrations of cloud condensation nuclei (CCN) from a few hundred up to one thousand cm^{-3} can strongly affect cloud microphysics (McFiggans et al., 2006; Reutter et al., 2009; Koren et al., 2014). Future expansion of cities and population throughout the basin can be expected to alter particle concentrations, and changes in cloud properties can be expected.

The Observations and Modeling of the Green Ocean Amazon (GoAmazon2014/5) Experiment was motivated by the need to gain a better understanding of aerosol–cloud–precipitation interactions and processes over the largest tropical rain forest on Earth. GoAmazon2014/5 sought to advance the goal of understanding how the chemical, hydrological, energy, and ecosystem cycles of the basin function today and how they might evolve under scenarios of future stress and pollution. The experiment assembled a network of observation sites to intercept both background air of the Amazon basin and pollution from the Manaus metropolis in the central region of Brazil (Fig. 1). Manaus, situated at the confluence of the Black River (Rio Negro) with the Solimões river, which together form the Amazon river, is an isolated urban region of over 2 million people (IBGE, 2015). The city has been a free trade zone since 1967 to encourage economic development, leading to the presence today of hundreds of local and global manufacturing companies. Most of the manufactured products are shipped thousands of kilometers by boat to the consumers in the southern states of Brazil. Outside of the city there is natural forest for over 1000 km in every direction. In this context, the airshed intersecting the GoAmazon2014/5 research sites downwind of Manaus oscillated between (i) one of the most natural continental sites on Earth and (ii) one characterized by the interactions of the pollution emissions of a tropical metropolis with the natural emissions of the rain forest. GoAmazon2014/5 was designed to explore cloud–aerosol–precipitation interactions over a tropical rain forest for which contrasting conditions of clean compared to polluted conditions were clearly and regularly delineated. The most heavily instrumented research site ("T3") of GoAmazon2014/5 was 70 km downwind of Manaus. Under the day-to-day variability in the meteorology, both clean and polluted air masses, mixed to variable degrees, arrived at T3. The pollution plume from Manaus

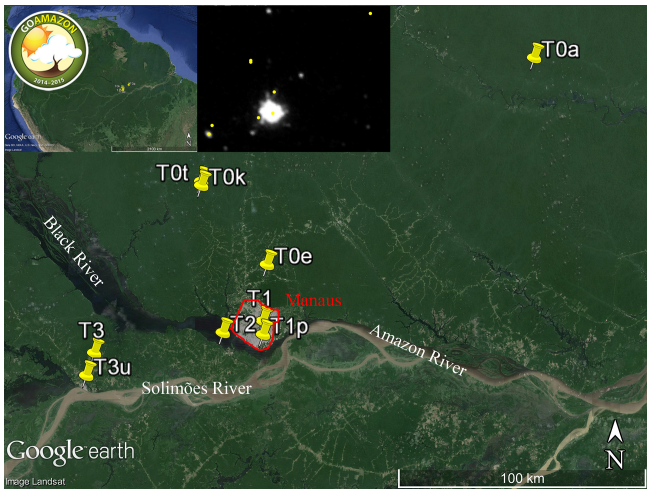

Figure 1. Locations of GoAmazon2014/5 research sites in the environs of the city of Manaus (−3.1°, −60.0°) in the state of Amazonas in the country of Brazil. Table 1 provides further information on the labeled sites. Manaus is located at the confluence of the Black River (Rio Negro) with the Solimões river, which together form the Amazon river. The map rectangle is drawn from (−3.66°, −60.92°) in the southwest to (−1.91°, −58.58°) in the northeast. The left inset shows the location of the experimental domain within South America. For prevailing winds, Manaus is on the order of 1200 (IOP1) to 1600 km (IOP2) from the South Atlantic. The right inset shows nighttime illumination in the environs of the city of Manaus for the year 2010. Figure S1 in the Supplement provides an expanded view of the regional nighttime illumination.

thus served as a laboratory for investigating perturbations to natural processes.

The regular synoptic changes between the wet and dry seasons offered an additional important scientific contrast. In the wet season, the Manaus plume aside, the Amazon basin is one of the cleanest continental regions on Earth (Andreae, 2007; Martin et al., 2010a). The particle population is in dynamic balance with the ecosystem (which produces them directly and indirectly) and the hydrologic cycle (which removes them). In the dry season, biomass burning is prevalent throughout the basin. The most intense burning and atmospheric perturbations take place at the southern and eastern edges of the vast forest. Local fire emissions as well as basin-wide background pollution also affect the Manaus region during this time period. Wet deposition also decreases during the dry season. As a result of these spatial and temporal differences, cloud–aerosol–precipitation interactions are significantly different between the two seasons (Andreae et al., 2004; Feingold et al., 2005; Artaxo et al., 2013).

The original use of the expression "green ocean" was related to the similarities in aerosol particle concentrations and cloud microphysics between the Amazon basin and remote oceanic regions during clean periods of the wet season (Williams et al., 2002). The expression, in reference to Green Ocean Amazon ("GoAmazon" for short) or "Observations and Modeling of the Green Ocean Amazon" (long version), has acquired a more general meaning to refer to the energy, water, and chemical cycles over the vast, mostly green-colored Amazon rain forest.

The anticipated publications for this special issue about GoAmazon2014/5 can be broadly categorized as related to (1) the aerosol life cycle, (2) the cloud life cycle, (3) cloud–aerosol–precipitation interactions, and (4) terrestrial ecosystems. The publications can be largely grouped as focusing on one or more of the following topics:

1. (a) perturbations of atmospheric composition and atmospheric oxidant cycle due to human activities in tropical continental regions, including interactions with biogenically produced volatile organic compounds; (b) associated influences on the number concentration, the mass concentration, the size distribution, and the optical, cloud-forming, and ice-nucleating properties of aerosol particles.

2. (a) the evolution of storms over tropical rain forests in the dry season (i.e., intense and relatively isolated storms) compared to the wet season (i.e., less intense but more widespread storms); (b) the daily transition in cloud development from shallow to deep convection, with comparison and understanding between tropical and other environments.

3. (a) effects of aerosol particles on clouds, precipitation, and lightning across a range of clean and polluted conditions; (b) the connections to aerosol direct, semi-direct, and indirect radiative effects.

4. (a) identities, amounts, and seasonal patterns of emissions of biogenic volatile organic compounds (BVOCs); (b) the controls on the fraction of assimilated carbon that is allocated to the production and emission of BVOCs.

This introduction to the special issue presents the objectives and motivation of the GoAmazon2014/5 experiment. It also provides a description of the field sites, the environmental conditions during the two Intensive Operating Periods (IOPs), and the context of the Manaus metropolis in the center of the largest rain forest on Earth.

2 Experimental design

The GoAmazon2014/5 Experiment took place in the environs of Manaus in the central region of the Amazon basin. Manaus, a city presently of over 2 million people and expanding rapidly, is an isolated urban region within the surrounding rain forest (Fig. 1). It is large enough to have an urban island heat effect of up to 3 °C relative to the surrounding forest (de Souza and dos Santos Alvalá, 2014).

Several important geographic features include the confluence of two large rivers, an urban landscape, and undulating land relief (50 to 200 m) that affects its daily meteorological cycles (dos Santos et al., 2014; Tanaka et al., 2014). GoAmazon2014/5 measurements were made from 1 January 2014 through 31 December 2015. Two Intensive Operating Periods, including aircraft and additional personnel and instrumentation at the ground sites, took place in the wet and dry seasons of 2014. GoAmazon2014/5 IOP1 took place from 1 February to 31 March 2014, and GoAmazon2014/5 IOP2 was active from 15 August to 15 October 2014. There were nine ground stations in and around Manaus as well as coordinated flights by research aircraft. The rationale for the use of the multiple platforms was to characterize the Amazonian atmosphere under varying degrees of urban influence and photochemical processing.

2.1 Site and aircraft descriptions

The locations of Manaus and the nine research sites are shown in Fig. 1. The latitude–longitude coordinates of each site are listed in Table 1. The sites range from time points zero (T0) upwind of the pollution, through time points one (T1) and two (T2) closer to the pollution sources, to time points three (T3) furthest downwind of the pollution. Instrumentation at each site, including the aircraft, is catalogued in Tables S1 to S13 in the Supplement. The scope and duration of the data sets that were collected by this combined set of instrumentation represents a new milestone for the study of climate and air quality in the Amazon basin.

Site T0a was the Amazonian Tall Tower Observatory (ATTO) (Andreae et al., 2015). Although the site has been active since 2012, the 325 m tall tower (inaugurated in August 2015) had not yet been completed during the IOPs of GoAmazon2014/5. Measurements were instead made from two 80 m towers at the site. Site T0e was located at a branch of the Brazilian Agricultural Research Corporation (EMBRAPA) about 10 km beyond the northern limits of the Manaus metropolitan area (Barbosa et al., 2014). Sites T0k and T0t were situated in the Cuieiras Biological Reserve ("ZF2") that has been a central part of Amazonian ecology and climate studies for over 20 years. In particular, T0k was the tower "K34" that has been the centerpiece of the Large-Scale Biosphere–Atmosphere (LBA) experiment since its construction in 1999 (Araújo et al., 2002). Site T0t was tower "TT34" established for the Amazonian Aerosol Characterization Experiment (AMAZE-08) in 2008 (Martin et al., 2010b). The T0 sites were typically upwind of Manaus so that the pollution plume was not present most of the time. In all cases, however, except possibly for T0a, the local winds did occasionally transport some pollution to these sites (Chen et al., 2015).

Within Manaus, site T1 was a tower in a forested section of the campus of the National Institute of Amazonian Research. Site T1p was located at the military airport at Ponta Pelada in Manaus. Site T2 consisted of a research container placed at a hotel on the western edge of the Black River and just across the river from Manaus (J. Brito, personal communication, 2015). It sampled the fresh Manaus pollution plume across approximately 8 to 11 km of river width depending on the prevailing wind direction. Site T3u was located on the regional campus of Amazonas State University in Manacapuru.

The most comprehensively instrumented site of GoAmazon2014/5 was T3. For 24 months, a suite of containers representing the Atmospheric Radiation Measurement (ARM) Climate Research Facility of the United States Department of Energy operated at T3. This facility included the ARM Mobile Facility One (AMF-1) and the ARM Mobile Aerosol Observing System (MAOS) (Mather and Voyles, 2013). There were four additional containers of instrumentation deployed by university investigators and other scientists during the two IOPs. The T3 site was located 70 km downwind of Manaus, representing several hours of air travel time depending on the daily wind speeds. It was a pasture site of 2.5 km by 2 km situated 2 km to the north of a lightly traveled two-lane road (AM-070) that connects Manaus to Manacapuru. Manacapuru was 10 km downwind of T3 to the southwest.

Two aircraft, a low-flying G-159 Gulfstream I (G-1) (Schmid et al., 2014) that mostly sampled the atmospheric boundary layer and low clouds and a high-flying Gulfstream G550 (HALO) (Wendisch et al., 2016) that mostly observed the free troposphere, collected data during the two IOPs. The flight tracks of HALO appear in Wendisch et al. (2016), constituting 14 research flights, mostly in the mid- and upper troposphere, during IOP2. The domain of flights was across a large part of the Amazon basin. There were two dedicated flights coordinated with the G-1 aircraft, including for instrument comparison. The G-1 carried out 16 flights in IOP1 and 19 flights in IOP2, mostly in the late morning and early afternoon (local time). Figure 2 shows all flight tracks of the G-1. Figures S2 and S3 segregate the tracks by altitude. Other than a few flight missions set up to sample background conditions, the flight tracks shown in Fig. 2 represent a synopsis of the actual location of the Manaus pollution plume on specific days. The flight tracks show that easterly winds carried the plume westward over the rain forest. On a given day, flight plans were filed in the early morning based on boundary layer winds sampled by radiosondes as well as on the forecasted location of the pollution plume. A plume forecast was prepared using the CATT-BRAMS model (Coupled Aerosol and Tracer Transport model to the Brazilian developments on the Regional Atmospheric Modelling System) (Freitas et al., 2009). In some cases, adjustments to the flight plans were made during flight once the instrumentation had identified the actual location of the daily plume.

Table 1. Names and locations of research sites and platforms deployed in GoAmazon2014/5. Other common names, as well as the relative distances and angles from T1 (National Institute of Amazonian Research, INPA), are also listed.

		Location		Position relative to T1			
GoAmazon2014/5 reference	Other reference	Latitude	Longitude	Distance (km)	Direction (0° N)	Description	Reference
T0a	ATTO	−2.1466°	−59.0050°	151.4	45.8°	Forested site upwind of Manaus, 325 m tall tower (inaugurated Aug 2015)	Andreae et al. (2015)
T0e	EMBRAPA	−2.8942°	−59.9718°	22.5	4.3°	Pasture site north of Manaus	Barbosa et al. (2014)
T0k	K34, ZF2	−2.6091°	−60.2093°	59.4	335.5°	Closed canopy, forested site north of Manaus	Araújo et al. (2002)
T0t	TT34, ZF2	−2.5946°	−60.2093°	60.9	336.1°	Broken canopy, forested site north of Manaus	Martin et al. (2010b)
T1	INPA	−3.0972°	−59.9867°	n/a	n/a	On INPA campus in Manaus	
T1p	Ponta Pelada	−3.1461°	−59.9864°	5.4	179.6°	Ponta Pelada Airport (PLL)	
T2	Tiwa Hotel	−3.1392°	−60.1315°	16.8	253.9°	Adjacent to river, just downwind of Manaus; river width of 7.5 to 11.7 km depending on direction of prevailing winds	
T3	MAOS, AMF-1, Fazenda Agropecuária Exata	−3.2133°	−60.5987°	69.4	259.2°	Pasture site downwind of Manaus	Mather et al. (2014)
T3u	UEA	−3.2953°	−60.6282°	74.6	252.9°	On campus of Amazonas State University (UEA) in Manacapuru	
G-1	AAF, G-159 Gulfstream I	n/a	n/a	n/a	n/a		Schmid et al. (2014)
HALO	Gulfstream G550	n/a	n/a	n/a	n/a		Wendisch et al. (2016)

2.2 Climatology

In the middle of the Amazon basin, Manaus is situated in an attractive scientific location because the full range of basin meteorology can be encountered. Cold fronts, which typically occur in the southwest part of the basin (Rondônia), can reach further north and affect the meteorology of the central part of the basin, most often in June and July. Squall lines, which are frequent in the eastern portion of the basin, also penetrate and propagate from the South Atlantic to the middle of the basin (Greco et al., 1990; Cohen et al., 1995; Alcântara et al., 2011), often leading to late night or early morning precipitation in Manaus (Machado et al., 2004). Organized synoptic convective events are most common at the start and the end of the wet season. These events are caused in large part by a monsoon circulation that shifts the ITCZ southward over Manaus and by squall lines that originate near the coast and propagate to the central region of the basin. A consequence of these dual synoptic perturbations is that the number of organized synoptic convective events per month is high in Manaus: around six during March and three during October (Machado et al., 2004).

The cloud cover and rainfall around Manaus is lowest in July and August during the central period of the dry season and highest in February and March in the midst of the wet season. Although seasonal variation in convective available potential energy (CAPE) is small, as is typical for rain forest close to the equator, rainfall in the wet season is more continuous but less intense compared to the dry season. The transition period between dry and wet seasons and the onset of the wet season are the time periods of maximum intensity for convection. Little seasonal variation in CAPE yet large variation in cloud cover and rainfall taken together imply that small perturbations in large-scale circulation in this region can possibly drive dramatic changes in rainfall.

2.3 Air pollution sources in metropolitan Manaus

Major sources of air pollution from Manaus include the vehicle fleet, power plants, and industrial activities, all of which are increasing annually. The population of Manaus grew from 1.5 million in 2004 to 2.0 million in 2014. Measured by percent growth, Manaus was the fastest growing major Brazilian city during this time period (IBGE, 2015). Manaus accounts for 80 % of the economic activity of the state of Amazonas.

In regard to the vehicle fleet, in December 2014 there were 622 675 vehicles registered in Manaus (DENATRAN, 2015). Outside of Manaus, there were an additional 133 088 vehicles in the state of Amazonas. For comparison, 10 years earlier (December 2004), there were 242 893 registered vehicles in Manaus, meaning a 250 % increase in the fleet from 2004 to 2014. In 2014, 255 758 registered vehicles used alcohol or gasoline, 281 811 consumed gasoline only, 54 158 were powered by diesel, and 30 948 employed another fuel or were unclassified. There were 326 806 passenger vehicles,

Figure 2. Flight tracks of the G-1 aircraft during **(a)** IOP1 and **(b)** IOP2 for all altitudes. The flight periods were from 22 February to 23 March 2014 in IOP1 and 6 September to 4 October 2014 in IOP2. The flight tracks grouped by altitude appear in Figs. S2 and S3.

150 127 motorcycles, 91 099 pickups, 28 285 trucks, 10 688 buses, and 15 690 vehicles of other types.

Electricity in Manaus is largely produced by the combustion of fossil fuels. In 2013, the power plants consumed 2.5×10^8 kg of fuel oil (providing 14 % of electricity produced), 1.3×10^9 m^3 of natural gas (55 %), and 6.1×10^8 L of diesel (31 %) (A. Medeiros, personal communication, 2015). The nominal installed capacity was 1.5 GW for fossil fuel power plants (Eletrobras, 2013). The locations of the plants in the urban region are shown in Fig. S4. The consumption of fossil fuels was complemented by a hydroelectric power plant (250 MW), which has operated in Balbina to the north of the city since 1989. Following the opening in November 2009 of a gas pipeline (661 km) from Urucu to Manaus and passing through Manacapuru, the fuel matrix for electricity production has been shifting from a historical reliance on sulfur-laden fuel oil and diesel to one having an increasing fraction of natural gas.

In addition to Manaus, important but less consequential sources of air pollution include multiple small municipalities along the Amazon river extending hundreds of kilometers to the east all the way to the South Atlantic. Between Manaus and T3, there are dozens of small brick factories (Fig. S5). These factories nearly exclusively use wood to fire the kilns (B. Portela, personal communication, 2015). Site T2 was impacted by these factories when well-known daily patterns of local river breezes transported air masses from the west (direction opposite to Manaus) (G. Cirino, personal communication, 2015) (Silva Dias et al., 2004; Trebs et al., 2012; dos Santos et al., 2014). With respect to T3, although the simulated wind trajectories at times passed near and through the locations of these factories, elevated concentrations of biomass burning tracers such as acetonitrile or levoglucosan were rare for the data sets of IOP1, suggesting that brick factory emissions did not have a significant influence on measurements at T3 most of the time (S. de Sá, personal communication, 2015). With respect to background air entering the Manaus region, the pollution from the small municipalities along the Amazon river as well as eastern coastal cities can become important in the dry season because of prevailing easterly winds during that season. Biomass burning also takes place throughout the basin, especially along the eastern and southern edges of the forest during the dry season, and can be an important source of regional pollution.

In 2001, the pollution plume from Manaus was characterized in transect flights by Kuhn et al. (2010). At that time, the plume consisted of high concentrations of oxides of sulfur, oxides of nitrogen, submicron aerosol particles, and soot, among other pollutants. Ozone was produced by photochemical reactions in the plume (Trebs et al., 2012). The width of the urban plume was 20 to 25 km, on the order of the size of the city itself.

3 Mesoscale and synoptic meteorology during the Intensive Operating Periods

3.1 IOP1

The account of mesoscale and synoptic meteorology is based on soundings as well as satellite observations. The trade winds carried equatorial air from the South Atlantic into the Amazon basin. Fourteen-day back trajectories, originating 100 m above Manaus, are grouped together and shown in Fig. 3a. Manaus (−3.1°) was typically under air masses coming from the Northern Hemisphere during IOP1 because of the southern positioning of the ITCZ during this time period.

Time series of altitude profiles of winds and relative humidity based on soundings launched at the T3 site, as well as a time series of regional rainfall based on retrievals from a radar at T3p, are presented in Fig. 4. Northeasterly winds

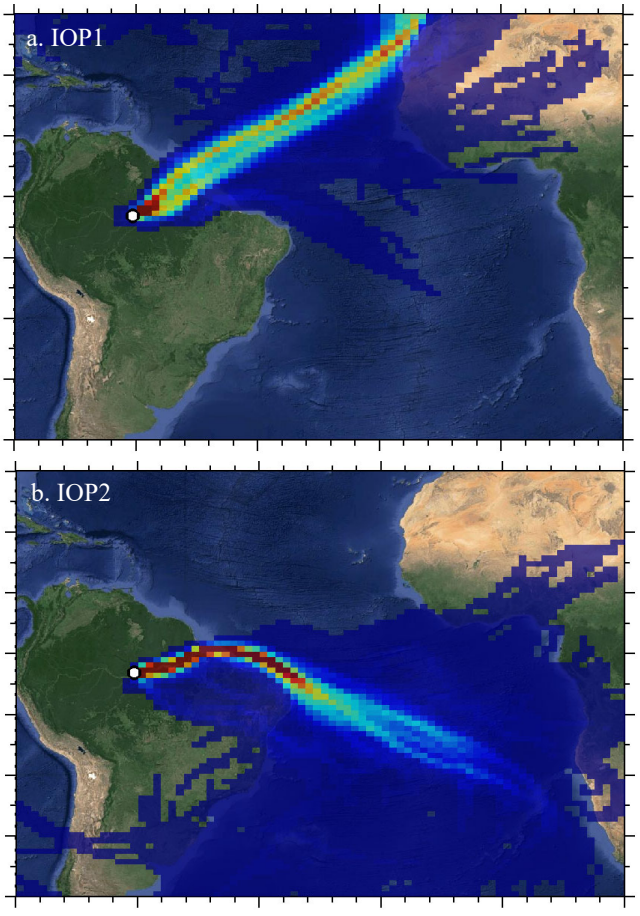

Figure 3. Fourteen-day back trajectories initialized at 100 m above T3 during **(a)** IOP1 and **(b)** IOP2. Meteorological fields were from the $1^\circ \times 1^\circ$ Global Data Assimilation System (GDAS). Source: http://www.arl.noaa.gov/HYSPLIT_info.php; last access: 15 August 2015.

prevailed in the atmospheric boundary layer of the Manaus region (Fig. 4a1 and a2). Regular and strong precipitation events are apparent in the time series of daily rainfall amounts (Fig. 4a3). Deep tropospheric moistening because of regular large rain events is apparent (Fig. 4a4).

The precipitation climatology for 2000–2014 and the associated weather anomalies are shown in Fig. 5a across a broad region of the Amazon basin in the wet season. A band of high precipitation from the South Atlantic to the central region of the basin accompanied squall lines that originated at the coast and propagated into the basin (Fig. 5a1). The maximum runs along the ITCZ. The precipitation anomalies, meaning the precipitation during the IOP compared to that of the 15-year climatology during that same period, were positive along the general trajectory of winds from the ocean coast to Manaus (Fig. 5a2). Positive anomalies were consistent with the discharges of the Madeira river, the main southern tributary to the Amazon river, which were 74 % higher than normal. The maximum level (June) of the Black River at Manaus in 2014 corresponded to the fifth highest during 113 years of records (Espinoza et al., 2014). Figure 5a2 also suggests that regions of strong positive anomalies in rainfall were associated with nearby regions of negative anomalies, suggesting an importance of mesoscale circulations of various types (e.g., forest–pasture, river breeze, and topography). On the synoptic scale, there was an intense warm anomaly in sea surface temperature (SST) in the southern South Atlantic and a weaker cold anomaly in the northern and equatorial South Atlantic (Fig. S6a). This anomaly in the SST gradient drove moisture transport from the South Atlantic toward the southwestern region of the Amazon basin. As a result, there was increased precipitation in the western part of the basin.

3.2 IOP2

During the dry season, the ITCZ shifted northward and the Manaus region was under air masses coming from the Southern Hemisphere (Fig. 3b). The trade winds carried air and moisture from the South Atlantic to the middle of the Amazon basin. Importantly (cf. Sect. 4), at times there was a recirculating pattern from the southern part into the middle section of South America. In the central region of the Amazon basin, strong easterlies prevailed in the surface boundary layer (Fig. 4b1 and b2). Compared to the wet season, rainfall was lower and the free troposphere was drier (Fig. 4b3 and b4). Moistening and higher levels of rain occurred in the final 10 days. Unlike IOP1, temperature anomalies over the South Atlantic during IOP2 were no longer significant (Fig. S6b). A strong warm anomaly was, however, present over the equatorial Pacific Ocean, corresponding to an El Niño development. The climatology of precipitation in the basin differs between the wet and dry seasons in both magnitude and geographical distribution (Fig. 5a1 compared to Fig. 5b1). There is in general little rainfall in the eastern part of the basin in the dry season, and, in particular for 2014, the precipitation anomaly was overall negative (Fig. 5b2), especially in September (not shown).

4 Regional and long-range transport of emissions during the Intensive Operating Periods

The wet season is viewed as a clean time period for background air, except for the episodic intrusions from Africa (Martin et al., 2010a). The dry season is sometimes alternatively referred to as the biomass burning season. During times of continental recirculation (cf. Sect. 3), biomass burning emissions from the southern edge of the forest transported south and southeast across the Atlantic coast of Brazil could in part return to the central Amazon. The backtrajectories in the dry season also passed reliably along the Amazon river, carrying the pollution of riparian communities and at

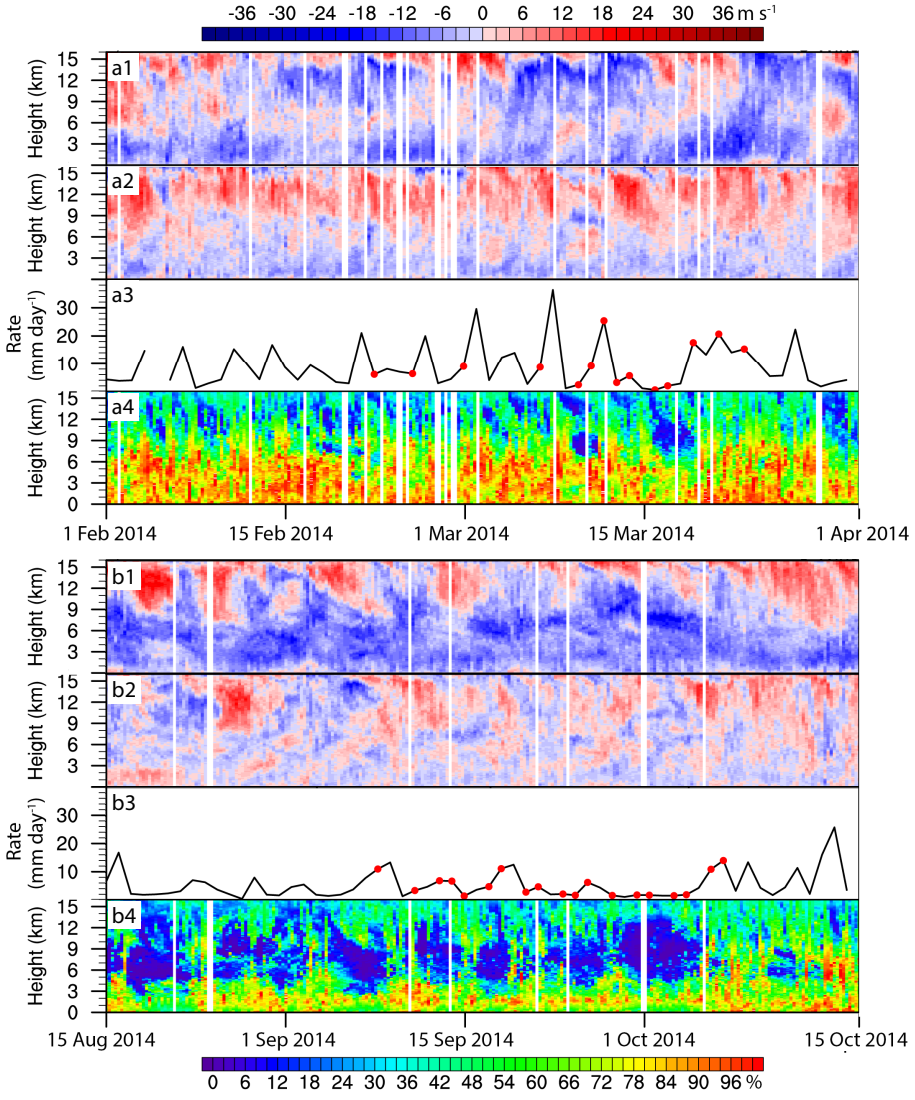

Figure 4. Time series of meteorological quantities during **(a)** IOP1 and **(b)** IOP2. (1) Altitude profile over T3 of wind velocities from the east (negative values; "*U*" winds). (2) Same as panel (1) but for wind velocities from the north (negative values; "*V*" winds). (3) Area-averaged rain rate in the Manaus region. Red circles indicate when the G-1 research aircraft flew a mission. (4) Altitude profile of relative humidity over T3. Scale bar of panels (1) and (2) is at the top of the figure. Scale bar for panel (4) is at the bottom of the figure. Data for wind and relative humidity were collected by four daily radiosondes launched at T3, and rows 1, 2, and 4 were prepared by interpolation of these data sets. Precipitation rates were based on measurements by an S-band radar operated by the Amazon Protection System (SIPAM) at T1p for returns at a height of 2.5 km and within a range of 110 km. Other data sources: https://www.arm.gov/campaigns/amf2014goamazon; last access: 12 September 2015.

times of large cities in the coastal northeast of Brazil into the Manaus region.

Fire locations in the near field of the Manaus region as well as in the far field of South America are plotted in the upper and lower rows of Fig. 6, respectively, for each IOP. A breakdown by week is shown in Figs. S7 and S8. Near-field fires represent upwind locations requiring on the order of 1 day for transport to the Manaus region. Pollution from these fires can be expected to have the physical and chemical signatures of fresh emissions. Far-field fires represent upwind locations requiring several days or more for transport to the Manaus region. The signatures become significantly aged during transport to the Manaus region. Figure 6 generally shows a low incidence of fires during the wet season (IOP1) compared to a high incidence during the dry season (IOP2).

Concentrations and emissions of aerosol particles on a hemispheric scale can be visualized by satellite by maps of aerosol optical depth (AOD). Weekly maps are shown in Fig. S9 for the two IOPs. Dust and biomass burning emissions from equatorial Africa were transported episodically

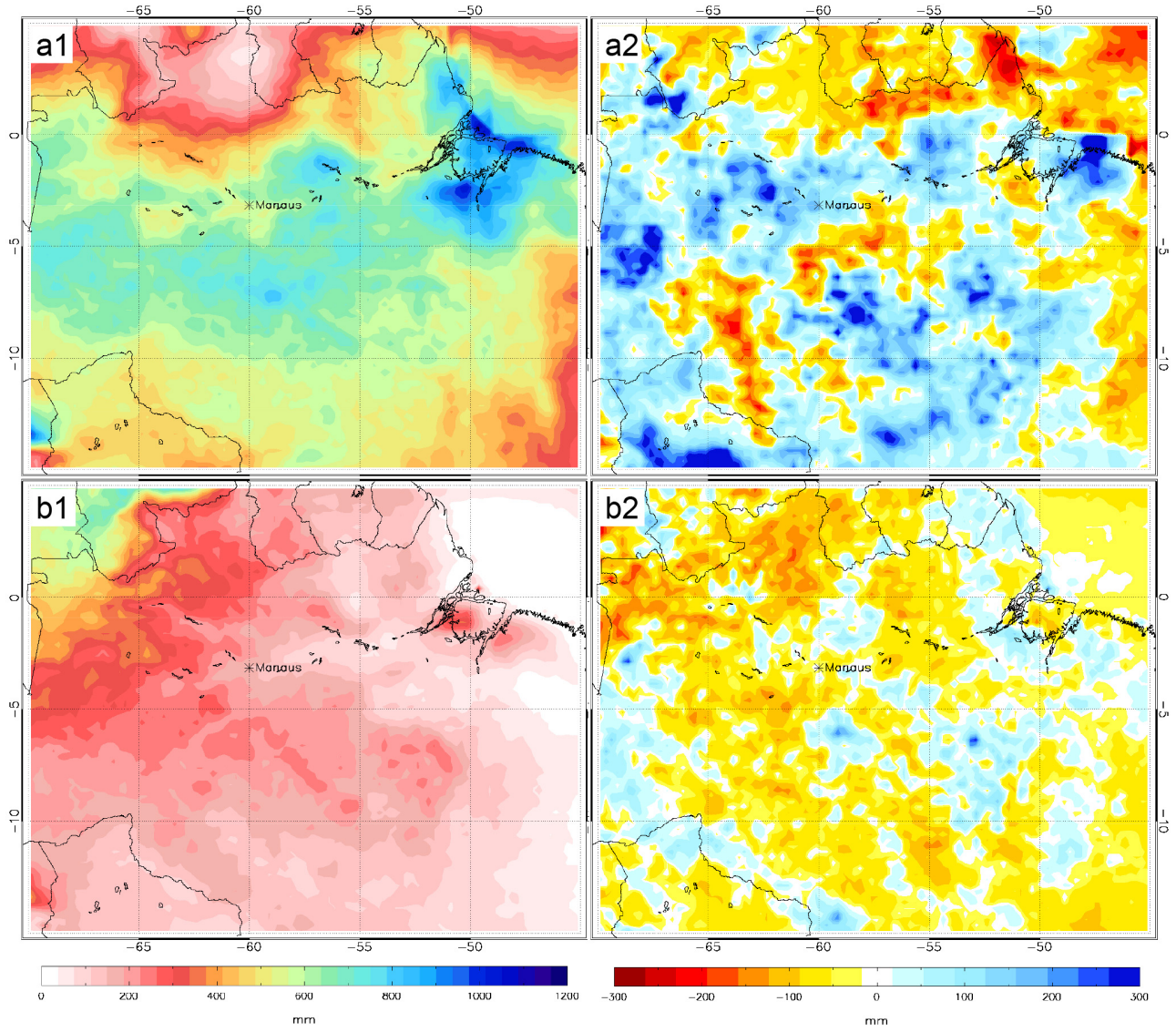

Figure 5. Mean accumulated precipitation (left column) from 2000 to 2014 throughout the Amazon basin based on the Tropical Rainfall Measuring Mission (TRMM) satellite and the Multi-Satellite Precipitation Analysis (TMPA) product (version 7 of the 3B42 algorithm). Anomaly of 2014 (right column) compared to the mean of 2000 to 2014. Results are shown for time periods of (top row) IOP1 and (bottom row) IOP2. Source: ftp://meso-a.gsfc.nasa.gov/pub/trmmdocs/3B42_3B43_doc.pdf; last access: 12 September 2015.

into the central Amazon, as explained by the southern positioning of the ITCZ during this time period. By comparison, during IOP2 these emissions passed northward to the Caribbean, as explained by the northward shift of the ITCZ during this time period. During IOP2, there were two regions of intense biomass burning. The first was the central region of South America, representing the burning edge of the Amazon rain forest and called the "arc of deforestation". Recirculation patterns for the dry season can transport a portion of these emissions to the central part of the Amazon basin where Manaus is located. The second region of biomass burning was the central part of Africa. Emissions from both of these regions arrived into the central region of the Amazon basin during IOP2, as can be inferred by an overlay of the backtrajectories apparent in Fig. 3 and the emissions and transport implied by the aerosol optical depth in Fig. S9. Although mass concentrations were greatly reduced during transport, the central Amazon represents quite clean baseline conditions so that even relatively small amounts of imported emissions (compared to the source regions) can have a regionally dominant effect compared to the otherwise clean receptor region.

In summary, the GoAmazon2014/5 Experiment focused on the complex interactions among vegetation, atmospheric

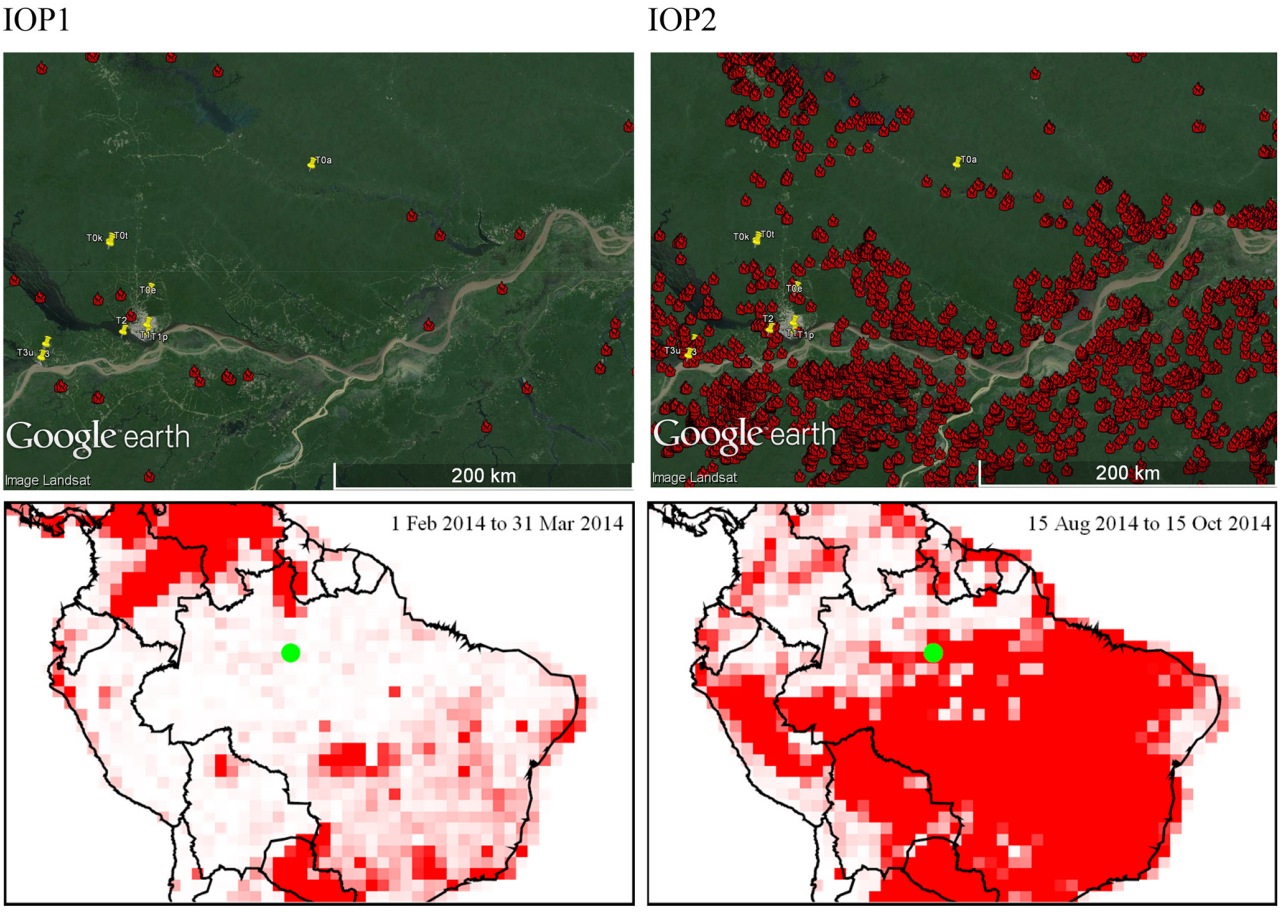

Figure 6. Satellite-based detection of fires (top) on the regional scale and (bottom) on the scale of South America. Left and right columns represent periods of IOP1 and IOP2, respectively. On the regional scale, each fire icon indicates the detection of one fire event during the 2-month observation period of each IOP. The yellow markers indicate the locations of GoAmazon2014/5 research sites (cf. Fig. 1). On the scale of South America, the color scaling in red runs from 0 to 100 fire events detected in a $1° \times 1°$ grid box during the 2-month observation period of each IOP. Some grid boxes have more than 100 events. The green point represents the location of Manaus. Source: http://www.dpi.inpe.br/proarco/bdqueimadas/; last access: 7 August 2015.

chemistry, and aerosol production and their connections to aerosols, clouds, and precipitation. It sought to understand how aerosol and cloud life cycles were influenced by pollutant outflow from a large city in the tropical rain forest, particularly the susceptibility of the biosphere and atmosphere to human activities, for a wide range of synoptic and environmental conditions. It was driven by the need to develop a knowledge base of data, processes, and mechanisms for inclusion in models of different types and scales. The intended future legacy of GoAmazon2014/5 is that more accurate predictions (embedded in models) should be developed of how the present-day functioning of energy, carbon, and chemical flows in the Amazon basin might change, both due to external forcing on the basin from global climate change and internal forcing from past and projected economic development in the basin. There can be future changes in direct, semi-direct, and indirect radiative forcing, energy distributions, regional climate, ecosystem functioning, and feedbacks to global climate.

In conjunction with the introduction presented herein, research results and findings of GoAmazon2014/5 appear in the articles of this special issue. The special issue is open for new submissions for 3 years. Overview articles are planned for summarizing and synthesizing the findings of the papers of the special issue. These planned overviews encompass the several objectives of GoAmazon2014/5.

The Supplement related to this article is available online at doi:10.5194/acp-16-4785-2016-supplement.

Acknowledgements. Institutional support was provided by the Central Office of the Large Scale Biosphere Atmosphere Experiment in Amazonia (LBA), the National Institute of Amazonian

Research (INPA), the National Institute for Space Research (INPE), Amazonas State University (UEA), and the Brazilian Space Agency (AEB). We acknowledge the Atmospheric Radiation Measurement (ARM) Climate Research Facility, a user facility of the United States Department of Energy, Office of Science, sponsored by the Office of Biological and Environmental Research, and support from the Atmospheric System Research (ASR) program of that office. Funding was obtained from the United States Department of Energy (DOE), the Amazonas State Research Foundation (FAPEAM), the São Paulo State Research Foundation (FAPESP), the Brazil Scientific Mobility Program (CsF/CAPES), the United States National Science Foundation (NSF), the German Max Planck Society (MPG), the German Research Foundation (DFG), and the German Aerospace Center (DLR). HALO flew as part of the coordinated ACRIDICON-CHUVA Experiment. The research was conducted under scientific licenses 001030/2012-4, 001262/2012-2, and 00254/2013-9 of the Brazilian National Council for Scientific and Technological Development (CNPq). A. Aiken, J. Brito, J. Fuentes, K. Jardine, J. Mather, A. Medeiros, R. A. J. Oliveira, C. Pöhlker, B. Portela, S. de Sá, B. Schmid, and S. Springston are acknowledged for assistance in the preparation of figures and tables.

Edited by: J. Allan

References

Alcântara, C. R., Silva Dias, M. A. F., Souza, E. P., and Cohen, J. C. P.: Verification of the role of the low level jets in Amazon squall lines, Atmos. Res., 100, 36–44, 2011.

Altaratz, O., Koren, I., Yair, Y., and Price, C.: Lightning response to smoke from Amazonian fires, Geophys. Res. Lett., 37, L07801, doi:10.1029/2010gl042679, 2010.

Andreae, M. O.: Aerosols before pollution, Science, 315, 50–51, 2007.

Andreae, M. O., Rosenfeld, D., Artaxo, P., Costa, A. A., Frank, G. P., Longo, K. M., and Silva-Dias, M. A. F.: Smoking rain clouds over the Amazon, Science, 303, 1337–1342, 2004.

Andreae, M. O., Acevedo, O. C., Araùjo, A., Artaxo, P., Barbosa, C. G. G., Barbosa, H. M. J., Brito, J., Carbone, S., Chi, X., Cintra, B. B. L., da Silva, N. F., Dias, N. L., Dias-Júnior, C. Q., Ditas, F., Ditz, R., Godoi, A. F. L., Godoi, R. H. M., Heimann, M., Hoffmann, T., Kesselmeier, J., Könemann, T., Krüger, M. L., Lavric, J. V., Manzi, A. O., Lopes, A. P., Martins, D. L., Mikhailov, E. F., Moran-Zuloaga, D., Nelson, B. W., Nölscher, A. C., Santos Nogueira, D., Piedade, M. T. F., Pöhlker, C., Pöschl, U., Quesada, C. A., Rizzo, L. V., Ro, C.-U., Ruckteschler, N., Sá, L. D. A., de Oliveira Sá, M., Sales, C. B., dos Santos, R. M. N., Saturno, J., Schöngart, J., Sörgel, M., de Souza, C. M., de Souza, R. A. F., Su, H., Targhetta, N., Tóta, J., Trebs, I., Trumbore, S., van Eijck, A., Walter, D., Wang, Z., Weber, B., Williams, J., Winderlich, J., Wittmann, F., Wolff, S., and Yáñez-Serrano, A. M.: The Amazon Tall Tower Observatory (ATTO): overview of pilot measurements on ecosystem ecology, meteorology, trace gases, and aerosols, Atmos. Chem. Phys., 15, 10723–10776, doi:10.5194/acp-15-10723-2015, 2015.

Araújo, A. C., Nobre, A. D., Kruijt, B., Elbers, J. A., Dallarosa, R., Stefani, P., von Randow, C., Manzi, A. O., Culf, A. D., Gash, J. H. C., Valentini, R., and Kabat, P.: Comparative measurements of carbon dioxide fluxes from two nearby towers in a central Amazonian rainforest: the Manaus LBA site, J. Geophys. Res.-Atmos., 107, LBA58.1–LBA58.20, 2002.

Artaxo, P., Rizzo, L. V., Brito, J. F., Barbosa, H. M. J., Arana, A., Sena, E. T., Cirino, G. G., Bastos, W., Martin, S. T., and Andreae, M. O.: Atmospheric aerosols in Amazonia and land use change: from natural biogenic to biomass burning conditions, Faraday Discuss., 165, 203–235, 2013.

Barbosa, H. M. J., Barja, B., Pauliquevis, T., Gouveia, D. A., Artaxo, P., Cirino, G. G., Santos, R. M. N., and Oliveira, A. B.: A permanent Raman lidar station in the Amazon: description, characterization, and first results, Atmos. Meas. Tech., 7, 1745–1762, doi:10.5194/amt-7-1745-2014, 2014.

Betts, A. K.: Evaluation of the diurnal cycle of precipitation, surface thermodynamics, and surface fluxes in the ECMWF model using LBA data, J. Geophys. Res., 107, 8045, doi:10.1029/2001jd000427, 2002.

Boisier, J. P., Ciais, P., Ducharne, A., and Guimberteau, M.: Projected strengthening of Amazonian dry season by constrained climate model simulations, Nature Climate Change, 5, 656–660, 2015.

Chen, Q., Farmer, D. K., Rizzo, L. V., Pauliquevis, T., Kuwata, M., Karl, T. G., Guenther, A., Allan, J. D., Coe, H., Andreae, M. O., Pöschl, U., Jimenez, J. L., Artaxo, P., and Martin, S. T.: Submicron particle mass concentrations and sources in the Amazonian wet season (AMAZE-08), Atmos. Chem. Phys., 15, 3687–3701, doi:10.5194/acp-15-3687-2015, 2015.

Cohen, J. C. P., Silva Dias, M. A. F., and Nobre, C. A.: Environmental conditions associated with Amazonian squall lines: a case study, Mon. Weather Rev., 123, 3163–3174, 1995.

Dai, A.: Precipitation characteristics in eighteen coupled climate models, J. Climate, 19, 4605–4630, 2006.

Dandin, P., Pontikis, C., and Hicks, E.: Sensitivity of a GCM to changes in the droplet effective radius parameterization, Geophys. Res. Lett., 24, 437–440, 1997.

Davidson, E. A., de Araújo, A. C., Artaxo, P., Balch, J. K., Brown, I. F., C. Bustamante, M. M., Coe, M. T., DeFries, R. S., Keller, M., Longo, M., Munger, J. W., Schroeder, W., Soares-Filho, B. S., Souza, C. M., and Wofsy, S. C.: The Amazon basin in transition, Nature, 481, 321–328, 2012.

DENATRAN: Departamento Nacional de Trânsito, available at: http://www.denatran.gov.br/frota2014.htm, last access: 6 August 2015.

de Souza, D. O. and dos Santos Alvalá, R. C.: Observational evidence of the urban heat island of Manaus City, Brazil, Meteorol. Appl., 21, 186–193, 2014.

dos Santos, M. J., Silva Dias, M. A. F., and Freitas, E. D.: Influence of local circulations on wind, moisture, and precipitation close to Manaus City, Amazon Region, Brazil, J. Geophys. Res.-Atmos., 119, 13233–13249, 2014.

Eletrobras: Management Report 2013: Electrobras Amazonas Energia, available at: http://www.eletrobrasamazonas.com/cms/wp-content/uploads/2011/02/Relatório-de-Gest~ao-Exercício-2013.pdf (last access: 28 August 2015), 2013.

Espinoza, J. C., Marengo, J. A., Ronchail, J., Carpio, J. M., Flores, L. N., and Guyot, J. L.: The extreme 2014 flood in south-western Amazon basin: the role of tropical-subtropical

South Atlantic SST gradient, Environ. Res. Lett., 9, 124007, doi:10.1088/1748-9326/9/12/124007, 2014.

Feingold, G., Jiang, H. L., and Harrington, J. Y.: On smoke suppression of clouds in Amazonia, Geophys. Res. Lett., 32, L02804, doi:10.1029/2004gl021369, 2005.

Freitas, S. R., Longo, K. M., Silva Dias, M. A. F., Chatfield, R., Silva Dias, P., Artaxo, P., Andreae, M. O., Grell, G., Rodrigues, L. F., Fazenda, A., and Panetta, J.: The Coupled Aerosol and Tracer Transport model to the Brazilian developments on the Regional Atmospheric Modeling System (CATT-BRAMS) – Part 1: Model description and evaluation, Atmos. Chem. Phys., 9, 2843–2861, doi:10.5194/acp-9-2843-2009, 2009.

Gloor, M., Brienen, R. J. W., Galbraith, D., Feldpausch, T. R., Schöngart, J., Guyot, J. L., Espinoza, J. C., Lloyd, J., and Phillips, O. L.: Intensification of the Amazon hydrological cycle over the last two decades, Geophys. Res. Lett., 40, 1729–1733, 2013.

Gonçalves, W. A., Machado, L. A. T., and Kirstetter, P.-E.: Influence of biomass aerosol on precipitation over the central Amazon: an observational study, Atmos. Chem. Phys., 15, 6789–6800, doi:10.5194/acp-15-6789-2015, 2015.

Greco, S., Swap, R., Garstang, M., Ulanski, S., Shipham, M., Harriss, R. C., Talbot, R., Andreae, M. O., and Artaxo, P.: Rainfall and surface kinematic conditions over central Amazonia during ABLE 2B, J. Geophys. Res.-Atmos., 95, 17001–17014, 1990.

IBGE: Instituto Brasileiro de Geografia e Estatística, available at: http://cidades.ibge.gov.br/, last access: 6 August 2015.

Keller, M., Bustamante, M., Gash, J., and Dias, P.: Amazonia and Global Change, Vol. 186, American Geophysical Union, Wiley, Washington, DC, 2009.

Koren, I., Altaratz, O., Remer, L. A., Feingold, G., Martins, J. V., and Heiblum, R. H.: Aerosol-induced intensification of rain from the tropics to the mid-latitudes, Nat. Geosci., 5, 118–122, 2012.

Koren, I., Dagan, G., and Altaratz, O.: From aerosol-limited to invigoration of warm convective clouds, Science, 344, 1143–1146, 2014.

Kuhn, U., Ganzeveld, L., Thielmann, A., Dindorf, T., Schebeske, G., Welling, M., Sciare, J., Roberts, G., Meixner, F. X., Kesselmeier, J., Lelieveld, J., Kolle, O., Ciccioli, P., Lloyd, J., Trentmann, J., Artaxo, P., and Andreae, M. O.: Impact of Manaus City on the Amazon Green Ocean atmosphere: ozone production, precursor sensitivity and aerosol load, Atmos. Chem. Phys., 10, 9251–9282, doi:10.5194/acp-10-9251-2010, 2010.

Lelieveld, J., Butler, T. M., Crowley, J. N., Dillon, T. J., Fischer, H., Ganzeveld, L., Harder, H., Lawrence, M. G., Martinez, M., Taraborrelli, D., and Williams, J.: Atmospheric oxidation capacity sustained by a tropical forest, Nature, 452, 737–740, 2008.

Lin, J. C., Matsui, T., Pielke, R. A., and Kummerow, C.: Effects of biomass-burning-derived aerosols on precipitation and clouds in the Amazon basin: a satellite-based empirical study, J. Geophys. Res.-Atmos., 111, D19204, doi:10.1029/2005JD006884, 2006.

Liu, Y. G. and Daum, P. H.: Anthropogenic aerosols – Indirect warming effect from dispersion forcing, Nature, 419, 580–581, 2002.

Machado, L. A. T., Laurent, H., Dessay, N., and Miranda, I.: Seasonal and diurnal variability of convection over the Amazonia: a comparison of different vegetation types and large scale forcing, Theor. Appl. Climatol., 78, 61–77, 2004.

Martin, S. T., Andreae, M. O., Artaxo, P., Baumgardner, D., Chen, Q., Goldstein, A. H., Guenther, A., Heald, C. L., Mayol-Bracero, O. L., McMurry, P. H., Pauliquevis, T., Pöschl, U., Prather, K. A., Roberts, G. C., Saleska, S. R., Silva-Dias, M. A., Spracklen, D. V., Swietlicki, E., and Trebs, I.: Sources and properties of Amazonian aerosol particles, Rev. Geophys., 48, RG2002, doi:10.1029/2008RG000280, 2010a.

Martin, S. T., Andreae, M. O., Althausen, D., Artaxo, P., Baars, H., Borrmann, S., Chen, Q., Farmer, D. K., Guenther, A., Gunthe, S. S., Jimenez, J. L., Karl, T., Longo, K., Manzi, A., Müller, T., Pauliquevis, T., Petters, M. D., Prenni, A. J., Pöschl, U., Rizzo, L. V., Schneider, J., Smith, J. N., Swietlicki, E., Tota, J., Wang, J., Wiedensohler, A., and Zorn, S. R.: An overview of the Amazonian Aerosol Characterization Experiment 2008 (AMAZE-08), Atmos. Chem. Phys., 10, 11415–11438, doi:10.5194/acp-10-11415-2010, 2010b.

Martins, J. A. and Silva Dias, M. A. F.: The impact of smoke from forest fires on the spectral dispersion of cloud droplet size distributions in the Amazonian region, Environ. Res. Lett., 4, 015002, doi:10.1088/1748-9326/4/1/015002, 2009.

Mather, J. H. and Voyles, J. W.: The ARM Climate Research Facility: A review of structure and capabilities, Bull. Am. Meteor. Soc., 94, 377–392, 2013.

McFiggans, G., Artaxo, P., Baltensperger, U., Coe, H., Facchini, M. C., Feingold, G., Fuzzi, S., Gysel, M., Laaksonen, A., Lohmann, U., Mentel, T. F., Murphy, D. M., O'Dowd, C. D., Snider, J. R., and Weingartner, E.: The effect of physical and chemical aerosol properties on warm cloud droplet activation, Atmos. Chem. Phys., 6, 2593–2649, doi:10.5194/acp-6-2593-2006, 2006.

Nobre, C. A., Sellers, P. J., and Shukla, J.: Amazonian deforestation and regional climate change, J. Climate, 4, 957–988, 1991.

Nobre, C. A., Obregón, G. O., Marengo, J. A., Fu, R., and Poveda, G.: Characteristics of Amazonian climate: main features, in: Amazonia and Global Change, American Geophysical Union, 149–162, 2009.

Pöschl, U., Martin, S. T., Sinha, B., Chen, Q., Gunthe, S. S., Huffman, J. A., Borrmann, S., Farmer, D. K., Garland, R. M., Helas, G., Jimenez, J. L., King, S. M., Manzi, A., Mikhailov, E., Pauliquevis, T., Petters, M. D., Prenni, A. J., Roldin, P., Rose, D., Schneider, J., Su, H., Zorn, S. R., Artaxo, P., and Andreae, M. O.: Rainforest aerosols as biogenic nuclei of clouds and precipitation in the Amazon, Science, 329, 1513–1516, 2010.

Reutter, P., Su, H., Trentmann, J., Simmel, M., Rose, D., Gunthe, S. S., Wernli, H., Andreae, M. O., and Pöschl, U.: Aerosol- and updraft-limited regimes of cloud droplet formation: influence of particle number, size and hygroscopicity on the activation of cloud condensation nuclei (CCN), Atmos. Chem. Phys., 9, 7067–7080, doi:10.5194/acp-9-7067-2009, 2009.

Rosenfeld, D., Lohmann, U., Raga, G. B., O'Dowd, C. D., Kulmala, M., Fuzzi, S., Reissell, A., and Andreae, M. O.: Flood or drought: how do aerosols affect precipitation?, Science, 321, 1309–1313, 2008.

Rosenfeld, D., Andreae, M. O., Asmi, A., Chin, M., de Leeuw, G., Donovan, D. P., Kahn, R., Kinne, S., Kivekäs, N., Kulmala, M., Lau, W., Schmidt, K. S., Suni, T., Wagner, T., Wild, M., and Quaas, J.: Global observations of aerosol-cloud-precipitation-climate interactions, Rev. Geophys., 52, 750–808, 2014.

Rotstayn, L. D. and Liu, Y. G.: Sensitivity of the first indirect aerosol effect to an increase of cloud droplet spectral dispersion with droplet number concentration, J. Climate, 16, 3476–3481, 2003.

Salati, E. and Vose, P. B.: Amazon basin: a system in equilibrium, Science, 225, 129–138, 1984.

Schmid, B., Tomlinson, J. M., Hubbe, J. M., Comstock, J. M., Mei, F., Chand, D., Pekour, M. S., Kluzek, C. D., Andrews, E., Biraud, S. C., and McFarquhar, G. M.: The DOE ARM aerial facility, B. Am. Meteorol. Soc., 95, 723–742, 2014.

Silva Dias, M. A. F., Silva Dias, P. L., Longo, M., Fitzjarrald, D. R., and Denning, A. S.: River breeze circulation in eastern Amazonia: observations and modelling results, Theor. Appl. Climatol., 78, 111–121, 2004.

Tanaka, L. M. d. S., Satyamurty, P., and Machado, L. A. T.: Diurnal variation of precipitation in central Amazon basin, Int J. Climatol., 34, 3574–3584, 2014.

Trebs, I., Mayol-Bracero, O. L., Pauliquevis, T., Kuhn, U., Sander, R., Ganzeveld, L., Meixner, F. X., Kesselmeier, J., Artaxo, P., and Andreae, M. O.: Impact of the Manaus urban plume on trace gas mixing ratios near the surface in the Amazon basin: implications for the NO-NO_2-O_3 photostationary state and peroxy radical levels, J. Geophys. Res., 117, D05307, doi:10.1029/2011jd016386, 2012.

Wang, H. and Fu, R.: The influence of Amazon rainfall on the Atlantic ITCZ through convectively coupled Kelvin waves, J. Climate, 20, 1188–1201, 2007.

Wendisch, M., Pöschl, U., Andreae, M. O., Machado, L. A. T., Albrecht, R., Schlager, H., Rosenfeld, D., Martin, S. T., Abdelmonem, A., Afchine, A., Araujo, A., Artaxo, P., Aufmhoff, H., Barbosa, H. M. J., Borrmann, S., Braga, R., Buchholz, B., Cecchini, M. A., Costa, A., Curtius, J., Dollner, M., Dorf, M., Dreiling, V., Ebert, V., Ehrlich, A., Ewald, F., Fisch, G., Fix, A., Frank, F., Futterer, D., Heckl, C., Heidelberg, F., Huneke, T., Jakel, E., Jarvinen, E., Jurkat, T., Kanter, S., Kastner, U., Kenntner, M., Kesselmeier, J., Klimach, T., Knecht, M., Kohl, R., Kolling, T., Kramer, M., Kruger, M., Krisna, T. C., Lavric, J. V., Longo, K., Mahnke, C., Manzi, A. O., Mayer, B., Mertes, S., Minikin, A., Molleker, S., Munch, S., Nillius, B., Pfeilsticker, K., Pohlker, C., Roiger, A., Rose, D., Rosenow, D., Sauer, D., Schnaiter, M., Schneider, J., Schulz, C., Souza, R. A. F. d., Spanu, A., Stock, P., Vila, D., Voigt, C., Walser, A., Walter, D., Weigel, R., Weinzierl, B., Werner, F., Yamasoe, M. A., Ziereis, H., Zinner, T., and Zoger, M.: The ACRIDICON–CHUVA campaign to study tropical deep convective clouds and precipitation using the new German research aircraft HALO, B. Am. Meteor. Soc., accepted, 2016.

Williams, E., Rosenfeld, D., Madden, N., Gerlach, J., Gears, N., Atkinson, L., Dunnemann, N., Frostrom, G., Antonio, M., Biazon, B., Camargo, R., Franca, H., Gomes, A., Lima, M., Machado, R., Manhaes, S., Nachtigall, L., Piva, H., Quintiliano, W., Machado, L., Artaxo, P., Roberts, G., Renno, N., Blakeslee, R., Bailey, J., Boccippio, D., Betts, A., Wolff, D., Roy, B., Halverson, J., Rickenbach, T., Fuentes, J., and Avelino, E.: Contrasting convective regimes over the Amazon: implications for cloud electrification, J. Geophys. Res.-Atmos., 107, 8082, doi:10.1029/2001jd000380, 2002.

Supplement of Atmos. Chem. Phys., 16, 4785–4797, 2016
http://www.atmos-chem-phys.net/16/4785/2016/
doi:10.5194/acp-16-4785-2016-supplement

Atmospheric Chemistry and Physics
Open Access
EGU

Supplement of

Introduction: Observations and Modeling of the Green Ocean Amazon (GoAmazon2014/5)

S. T. Martin et al.

Correspondence to: S. T. Martin (scot_martin@harvard.edu)

List of Supplementary Tables

Table S12. Instrumentation deployed on board the G1 (AMF) aircraft during the Intensive Operating Periods of GoAmazon2014/5.

Table S13. Instrumentation deployed on board the HALO aircraft during the second Intensive Operating Period of GoAmazon2014/5.

List of Supplementary Figures

Figure S1. Nighttime illumination in the environs of the city of Manaus (-3.1°, -60.0°) for the year 2010. The yellow points show the locations of the GoAmazon2014/5 research sites of Figure 1. Source: http://maps.ngdc.noaa.gov/viewers/dmsp_gcv4/ and http://ngdc.noaa.gov/eog/dmsp/downloadV4composites.html, accessed 12 August 2015.

Figure S2. Flight tracks of the G1 aircraft during IOP1 segregated by (a) 250 to 750 m above sea level, (b) 750 to 1250 m, (c) 1250 to 1750 m, and (d) above 1750 m.

Figure S3. Flight tracks of the G1 aircraft during IOP2 segregated by (a) 250 to 900 m above sea level, (b) 1000 to 2000 m, and (c) above 2000 m.

Figure S4. Locations of power plants in the environs of Manaus (orange pins). The location of a large refinery is also shown (blue pin). Yellow pins show the locations of some of the GoAmazon2014/5 research sites (cf. Figure 1). Source: personal communication, Adan Medeiros, 10 August 2015.

Figure S5. Locations of brick factories between Manaus (T1) and to the north of Manacapuru (T3). Source: personal communication, Bruno Portela, 8 September 2015.

Figure S6. Anomalies of sea surface temperature (SST) during (a) IOP1 and (b) IOP2. The climatology of 1981 through 2010 is the used as the reference for presentation of the anomalies in 2014 based on the NCEP/NCAR reanalysis. Source: http://rda.ucar.edu/datasets/ds090.0/, accessed 12 September 2015.

Figure S7. Satellite-based detection of fires on regional scale. Left and right columns represent periods of IOP1 and IOP2, respectively. Each fire icon indicates the detection of one fire event during the seven-day observation period. The yellow markers

indicate the locations of GoAmazon2014/5 research sites (cf. Figure 1). Source: http://www.dpi.inpe.br/proarco/bdqueimadas/, accessed 7 August 2015.

Figure S8. Satellite-based detection of fires on the scale of South America. Left and right columns represent periods of IOP1 and IOP2, respectively. Color scaling in red runs from 0 to 100 fire events detected in a 1° × 1° grid box during the seven-day observation period. Some grid boxes have more than 100 events. The green point represents the location of Manaus. Source: http://www.dpi.inpe.br/proarco/bdqueimadas/, accessed 7 August 2015.

Figure S9. Aerosol optical depth observed by the MODIS instrument on the AQUA satellite (eight-day composites, Collection 5). Left and right columns represent periods of IOP1 and IOP2, respectively. Color scaling is from an optical depth of 0.0 to 0.8. Black indicates regions over which optical depth was not retrieved, largely because of the high albedo of the Earth's surface in these regions. Source: http://modis-atmos.gsfc.nasa.gov/MYD08_E3/browse_c51.html, accessed 5 August 2015.

Instrument	Abbreviation	Data Available IOP1	Data Available IOP2	Investigator
Aerosol Chemical Speciation Monitor (Aerodyne)	ACSM	Yes	Yes	Artaxo
Scanning Mobility Particle Sizer (TSI)	SMPS	Yes	Yes	Artaxo
Condensation Particle Counter (Grimm, model 5412)	CPC	Yes	Yes	Pöhlker
Multiangle Absorption Photometer 5012 (Thermo, model 5012)	MAAP	Yes	Yes	Pöhlker
Aethalometer (Magee)	AE30	Yes	Yes	Artaxo
Nephelometer (Ecotech Aurora 3000)		Yes	Yes	Artaxo
Ultra-High Sensitivity Aerosol Spectrometer (DMT)	UHSAS	Yes	Yes	Pöhlker
Single Particle Soot Photometer (DMT)	SP2	Yes	Yes	Pöhlker
Size-Resolved Cloud Condesation Nuclei Counter (DMT)	Size-resolved CCNC	No	Yes	Artaxo/Pöhlker
Optical Particle Sizer (TSI, model 3330)	OPS	Yes	Yes	Pöhlker
Wide Range Aerosol Spectrometer (Grimm)	WRAS	No	Yes	Pöhlker
Wideband Integrated Bioaerosol Spectrometer (DMT)	WIBS-4	No	Yes	Su
Proton-Trasfer-Reaction Quadrupole Mass Spectrometer (Ionicon)	PTR-Q-MS	Yes	Yes	Kesselmeier
Picarro CRDS (Model G1302; S/N CKADS-018)		Yes	Yes	Lavric
Picarro CRDS (Model G1301; S/N CKADS-109)		Yes	Yes	Lavric
Chemolimuniscence NOx monitor (Ecotech CLD TR 780)	CLD	Yes	Yes	Sörgel
CO2 monitor (LI-COR 7000)		Yes	Yes	Sörgel
Ozone monitor (TEI 49 I)		Yes	Yes	Sörgel / Souza
Optical Fog Sensor (Eigenbrodt)		No	Yes	Pöhlker
Soil Heat Flux Sensor (HFP01, Hukseflux)		Yes	Yes	Araujo
Water Content Reflector (CS615, Campbell)		Yes	Yes	Araujo
Thermistor (108, Campbell)		Yes	Yes	Araujo
Pyranometer (CMP21 & CMP4, Kipp & Zonen)		Yes	Yes	Araujo
Quantum Sensor (PAR-LITE, Kipp & Zonen)		Yes	Yes	Araujo
Net radiometer (NR-LITE, Kipp & Zonen)		Yes	Yes	Araujo
UV radiometer (Kipp & Zonen, CUV5)		Yes	Yes	Araujo
Rain Gauge (TB4, Hydrological Services Pty. Ltd.)		Yes	Yes	Araujo
Termohygrometer (CS215, Rotronic Measurement Solutions)		Yes	Yes	Araujo
Barometer (PTB101B, Vaisala)		Yes	Yes	Araujo
2-D Sonic Anemometer (Windsonic, Gill)		Yes	Yes	Araujo
3-D Sonic Anemometer (Windmaster, Gill)		Yes	Yes	Araujo
IRGA (LI-7500A & LI7200, LI-COR)		Yes	Yes	Araujo

Table S1

Instrument	Abbreviation	Data Available		Investigator
		IOP1	IOP2	
Hg Monitor (TEKRAN)	Tekran	Yes	Yes	Artaxo
Nephelometer (Ecotech)	Neph_M9003	Yes	Yes	Artaxo
Multi filter shadow band radiometer (YesInc)	MFR	Yes	Yes	Barbosa
Sun Photometer (Cimel)	Aeronet	Yes	Yes	Artaxo
UV Raman Lidar (Raymetrics)	Lidar	Yes	Yes	Barbosa
24GHz Micro Rain Radar (Metek)	MRR	No	Yes	Barbosa
Laser precipitation monitor (Thies)	Disdro_Thies	Yes	Yes	Barbosa
Meteorological weather station (Davis)	MetDavis	No	No	Barbosa / Souza
Meteorological weather station (Thies)	MetThies	No	Yes	Barbosa
Meteorological weather station (Gill)	MetGill	No	Yes	Barbosa
NetR8 GNSS Receiver (Trimble)	GNSS	Yes	Yes	Barbosa
Precipitation Collector NSA 181/KE DURAN (Eigenbrodt)	Eigenbrodt	No	Yes	Barbosa
Meteorological weather station (Campbell)	MetCambpell	Yes	Yes	Machado
Passive Infraread Microwave radiometer MP3000 (Radiometrics)	MP3000	Yes	No	Machado
Parsivel Disdrometer (OTT)	Parsivel	Yes	No	Machado
IRGASON Integrated CO2 and H2O Open-Path Gas Analyzer and 3D Sonic Anem	FluxCampbell	Yes	Yes	Machado

Table S2

Instrument	Abbreviation	Data Available		Investigator
		IOP1	IOP2	
Proton tranfer reaction mass spectrometer	PTR-MS	Yes	Yes	Jardine
Gas chromatograph - mass spectrometter	GC-MS	Yes	Yes	Jardine
Proton tranfer reaction mass spectrometer	PTR-MS	No	Yes	Chamecki/Fuentes
Gas chromatograph - mass spectrometter	GC-MS	No	Yes	Chamecki/Fuentes
Sonic anemometers (10)		No	Yes	Chamecki/Fuentes
Water vapor gas analyzer	IRGA	No	Yes	Chamecki/Fuentes
Carbon dioxide gas analyzer	IRGA	No	Yes	Chamecki/Fuentes
Ozone gas analyzer		No	Yes	Chamecki/Fuentes
Sulfur dioxide gas analyzer		No	Yes	Chamecki/Fuentes
Carbon monoxide gas analyzer		No	Yes	Chamecki/Fuentes
Nitric oxide gas analyzer		No	Yes	Chamecki/Fuentes
Fast mobility particle sizer	FMPS	No	Yes	Chamecki/Fuentes
Cloud condensation nuclei counter	CCN counter	No	Yes	Chamecki/Fuentes
Picarro (CO, CO2, H2O)	CKADS	Yes	Yes	Jardine/Fuentes

Table S3

Instrument	Abbreviation	Data Available		Investigator
		IOP1	IOP2	
High-Resolution Time-of-Flight Aerosol Mass Spectrometer (Aerodyne Inc.)	HR-ToF-AMS	Yes	No	McFiggans
Proton-Trasfer-Reaction Quadrupole Mass Spectrometer (Ionicon)	PTR-Q-MS	Yes	No	McFiggans
Multiangle Absorption Photometer 5012 (Thermo)	MAAP	Yes	Yes	Artaxo
Nephelometer (TSI)		Yes	Yes	Artaxo
Tapered-Element Oscillating Microbalance	TEOM	No	Yes	Artaxo
Picarro (CO, CO2, H2O)	CKADS	Yes	Yes	Artaxo
Ozone	Thermo_49i	Yes	Yes	Artaxo
Four daily sondes at (-2.639°, -60.157°) (7.5 km to the southeast of T0t)		Yes	Yes	Machado

Table S4

Instrument	Abbreviation	Data Available		Investigator
		IOP1	IOP2	
Meteorological station	MetHOBO	Yes	Yes	Souza
Solar radiation and photosynthenitically active radiation	MetHOBO	Yes	Yes	Souza
Passive tubes for trace gases		No	Yes	Souza
PM2.5 Filter Sampler		No	Yes	Souza

Table S5

Instrument	Abbreviation	Data Available	
		IOP1	IOP2
Four daily radio sondes		Yes	Yes
S-band radar operated by the Amazon Protection System (SIPAM)		Yes	Yes

Table S6

Instrument	Abbreviation	Data Available IOP1	Data Available IOP2	Investigator
Proton-Trasfer-Reaction Quadrupole Mass Spectrometer (Ionicon)	PTR-Q-MS	Yes	Yes	Artaxo
Ozone Monitor 49i (Thermo)	O3 Monitor	Yes	Yes	Artaxo
SO2 Monitor 43i (Thermo)	SO2 Monitor	Yes	Yes	Artaxo
Cavity Attenuated Phase Shift NO2 Monitor (Aerodyne Inc.)	CAPS NO2	No	Yes	Artaxo
CO, N2O monitor (Los Gatos Research)	CO, NO2 LGR	Yes	Yes	Souza
Scanning Mobility Particle Sizer (TSI Inc.)	SMPS	Yes	Yes	Artaxo
Aerosol Chemical Speciation Monitor (Aerodyne Inc.)	ACSM	Yes	Yes	Artaxo
Multiangle Absorption Photometer 5012 (Thermo)	MAAP	Yes	Yes	Artaxo
Aethalometer (Magee Inc.)	7l - AE33	Yes	Yes	Artaxo
Nephelometer (Ecotech)	3-l Neph Aurora	Yes	Yes	Artaxo
Tapered Element Oscillating Microbalance 1405 (Thermo)	TEOM PM2.5 & PM10	No	Yes	Artaxo
Cloud Condensartion Nuclei Counter (Droplet Measurement Technologies)	Size-resolved CCNC	No	Yes	Artaxo

Table S7

Instrument	Abbreviation	Data Available IOP1	Data Available IOP2	Investigator
Disdrometer (Parsivel)		Yes	Yes	Machado
X-Band Radar		Yes	Yes	Machado
Micro Rain Radar	MRR	No	Yes	Machado
High-Resolution Time-of-Flight Aerosol Mass Spectrometer (Aerodyne Inc.)	HR-ToF-AMS	Yes	Yes	Alexander/Martin
Semi-Volatile Thermal Desorption Aerosol Gas Chromatograph	SV-TAG	Yes	Yes	Goldstein
Size-Resolved Cloud Condensation Nuclei Counter	SCCN	Yes	Yes	Wang
Harvard Rebound Apparatus	HBA	Yes	Yes	Martin
Oxidation Flow Reactor	OFR	Yes	Yes	Jimenez
Proton Transfer Reaction Time-of-Flight Mass Spectrometer	PTR-ToF-MS	Yes	Yes	Martin/MAOS
Proton Transfer Reaction Time-of-Flight Mass Spectrometer	PTR-ToF-MS	Yes	Yes	Guenther
Scanning Mobility Particle Sizer	SMPS	Yes	Yes	Jimenez
HOx Chemical Ionization Mass Spectrometer	HOx-CIMS	Yes	Yes	Kim
Picarro CRDS G2401 analyzer (CO, CO2, CH4)	Picarro	Yes	Yes	Jimenez
Medium Volume Filter Sampler, PM1 (MCV, S.A.)		Yes	Yes	Jimenez
Air Quality Monitoring 60 (O3)	AQM-60	Yes	Yes	Souza
Sequential Filter Sampler		Yes	Yes	Goldstein
Transmission electron microscope grip sampler	TEM grid sampler	Yes	Yes	Buseck
PM2.5 Filter Sampler		Yes	Yes	Godoi/Souza
Filter sampler (quartz and nuclepore)		Yes	Yes	Artaxo
Laser-induced flurescence	LIF	Yes	Yes	Keutsch
Micro-Orifice Uniform-Deposit Impactor	MOUDI	No	Yes	Laskin
Neutral cluster and Air Ion Spectrometer	NAIS	No	Yes	Petaja
Nano particle size distribution	NPSD	Yes	Yes	Kuang
Passive tubes for trace gases		Yes	Yes	Godoi/Souza
Particle Size Magnifier	PSM	No	Yes	Petaja
Laser Induced Phosphorescence	LIP	No	Yes	Keutsch
Thermal Desorption Chemical Ionization Mass Spectrometer	TD-CIMS	Yes	Yes	Smith
Precipication collection for chemical analysis		No	Yes	Pauliquevis
Solar radiation and photosynthenitically active radiation		Yes	Yes	Souza
Meteorological station		Yes	Yes	Souza

Table S8

Instrument	Abbreviation	Data Available	
		IOP1	IOP2
Aerosol Chemistry Speciation Monitor	ACSM	No	Yes
Aethalometer, 7-Wavelength	Aeth	Yes	Yes
CO, N2O and H2O Analyzer	CO/N2O/H2O	Yes	Yes
Condensation Particle Counter, Fine Mode	CPCf	Yes	Yes
Condensation Particle Counter, Ultrafine Mode	CPCu	No	No
Meteorology Sensor	Met	Yes	Yes
Nephelometer	Neph	Yes	Yes
Nephelometer, dry	NephDry	Yes	Yes
Oxides of Nitrogen Analyzer	NO/NOx/NOy	Yes*	Yes
Ozone Analyzer	O3	Yes	Yes
Photoacoustic Soot Spectrometer, 3-Wavelength	PASS-3	No	No
Particle Soot Absorption Photometer	PSAP	Yes	Yes
Proton Transfer Mass Spectrometer	PTRMS	Yes	Yes
Scanning Mobility Particle Sizer	SMPS	No	No
Single Particle Soot Photometer	SP2	Yes	Yes
SO2 Analyzer	SO2	No	Yes
Ultra-High Sensitivity Aerosol Spectrometer	UHSAS	Yes	Yes

*Only NO and NOy in IOP1

Table S9

Instrument	Abbreviation	Data Available IOP1	IOP2
Two-Channel Narrow Field of View Zenith Radiometer	2NFOV	Yes	No
Atmospheric Emitted Radiance Interferometer	AERI	Yes	Yes
Propeller Vane Wind Sensors	Anemometer	Yes	Yes
Black and White pyranometer, shaded, downwelling	B/W 8-48-SKY	Yes	Yes
Barometer	Barometer	Yes	Yes
Ceilometer Cloud Lidar	Ceilometer	Yes	Yes
Cloud Condensation Nuclei Counter	CCN	Yes	Yes
Continuous Light Absorption Photometer	CLAP	Yes	No
Condensation Particle Counter	CPC	Yes	Yes
Cimel Sunphotometer	CSPHOT	Yes	No
Doppler Lidar	DL	Yes	Yes
Eddy Correlation Flux Measurement System	ECOR	No	Yes
Infrared Thermometer Downlooking	IR Therm Grd	Yes	Yes
Infrared Thermometer Uplooking	IRT-Sky	Yes	Yes
ARM-Standard Meteorological Instrumentation at Surface	Met	Yes	Yes
Multi-Filter Radiometer	MFR	No	Yes
Multi-Filter Rotating Shadow Band Radiometer	MFRSR	Yes	Yes
Micropulse Lidar	MPL	No	Yes
Microwave Radiometer	MWR	Yes	Yes
Microwave Radiometer 3 Channel	MWR 3C	Yes	Yes
Microwave Radiometer High Frequency	MWR HF	No	No
Microwave Radiometer P	MWR P	No	No
Nephelometer	Neph	Yes	Yes
Nephelometer, wet	NephDry	No	Yes
Normally Incident Pyroheliometer: Installed and recording data	NIP	Yes	Yes
Optical Rain Gauge	ORG	No	No
Parsivel Present Weather detector	Parsivel2 disdrometer	No	No
Pyrogeometer, upwelling	PIR-GRND	Yes	Yes
Pyrogeometer, downwelling	PIR-SKY	Yes	Yes
Present Weather Detector	PWD	Yes	Yes
Particle Soot Absorption Photometer	PSAP	Yes	Yes
Precision Spectral Pyranometer, upwelling	PSP-GRND	Yes	Yes
Precision Spectral Pyranometer, downwelling	PSP-SKY	Yes	Yes
Radar Wind Profiler	RWP	Yes	Yes
Ka/W-band Scanning ARM Cloud Radar	SACR	No	No
Shortwave Array Spectroradiometer - 180 deg field of view	SAS-HE	Yes	Yes
Shortwave Array Spectroradiometer - Zenith pointing	SAS-ZE	Yes	Yes
Surface Energy Balance System	SEBS	Yes	No
Sound-based wind profiler	SODAR	Yes	Yes
Sonic Anemometer	Sonic	No	Yes
Tipping Bucket Rain Gauge	TB Rain Gauge	No	No
Total Sky Imager	TSI	No	No
Temperature and Humidity Sensor	T/RH	Yes	Yes
W-band (95 GHz) ARM Cloud Radar	WACR	Yes	Yes
Five daily radio sondes (0, 6, 12, 15 and 18 UTC)		Yes	Yes

Table S10

Instrument	Abbreviation	Data Available		Investigator
		IOP1	IOP2	
Disdrometer (Joss)		Yes	Yes	Machado
Disdrometer (Parsivel)		Yes	Yes	Machado
Rain Gauge		Yes	Yes	Machado
Microwave Radiometer (MP3000)		No	Yes	Machado
Micro Rain Radar	MRR	Yes	Yes	Machado
GPS-Based Integrated Water Vapor	IWV	Yes	Yes	Machado
Field Mill		Yes	Yes	Machado

Table S11

Instrument	Abbreviation	Data Available IOP1	IOP2
Global Positioning System (DSM 232)	GPS	Yes	Yes
Temperature (Rosemount E102AL)		Yes	Yes
Pressure (Rosemount 1201F1)		Yes	Yes
Gust Probe: Rosemount 1221F2 (3 units)		Yes	Yes
Chilled-mirror hygrometer (GE-1011B)		Yes	Yes
Tuneable Diode Laser Hygrometer	TDL-H	Yes	Yes
Aircraft Integrated Meteorological Measurement System	AIMMS-20	Yes	Yes
Video Camera P1347 (forward looking)		Yes	Yes
Video Camera P1344		Yes	Yes
Ultrafine Condensation Particle Counter (Model 3025A)	UCPC	Yes	Yes
Condensation Particle Counter (Model 3010)	CPC	Yes	Yes
Fast Integrated Mobility Spectrometer	FIMS	Yes	Yes
Ultra High Sensitivity Aerosol Spectrometer - Airborne	UHSAS-A	Yes	Yes
Passive Cavity Aerosol Spectrometer	PCASP	Yes	Yes
Particle/Soot Absorption Photometer	PSAP	Yes	Yes
Three-Wavelength Integrating Nephelometer (Model 3563)		Yes	Yes
High Resolution Aerosol Mass Spectrometer	HR-ToF-AMS	Yes	Yes
Cloud Condensation Nuclei Counter	CCN Counter	Yes	Yes
Optical Particle Counter (Model CI-3100)	OPC	Yes	Yes
Quadrupole Proton-Transfer-Reaction Mass Spectrometer	PTR-MS	Yes	Yes
N2O and CO concentrations (Los Gatos 23r)		Yes	Yes
Oxides of Nitrogen (Nox)		Yes	Yes
Ozone (Thermo Scientific Model 49i)		Yes	Yes
Picarro Cavity Ring Down System (Model G1301-m)	CRD	Yes	Yes
Multi Element Water content System (SEA WCM-2000)		Yes	Yes
High Volume Precipitation Spectrometer (Version 3)	HVPS-3	Yes	Yes
Two-Dimensional Stereo Probe	2D-S	Yes	Yes
Fast Cloud Droplet Probe	Fast-CDP	Yes	Yes
Cloud Droplet Probe (version 2)	CDP ver2	Yes	Yes
Cloud Particle Imager (version 2)	CPI ver2	Yes	Yes
Sunshine Pyranometer, shaded	SPN-1	Yes	Yes
Sunshine Pyranometer, unshaded (up and down looking)	SPN-1	Yes	Yes

Table S12

Instrument	Abbreviation	Data Available	
		IOP1	IOP2
Counter-flow Virtual Impactor Inlet	CVI inlet	No	Yes
Precipitation Imaging Probe	PIP	No	Yes
Cloud Combination Probe (Cloud ImagingProbe + Cloud Droplet Probe)	CCP (CIP + CDP)	No	Yes
Novel Ice EXpEriment - Cloud and Aerosol Particle Spectrometer	NIXE-CAPS	No	Yes
Small Ice Detector Probe (version 3)	SID-3	No	Yes
Microwave Temperature Profiler	MTP	No	Yes
Ultra High Sensitivity Aerosol Spectrometer - Airborne	UHSAS-A	No	Yes
Cloud and Aerosol Spectrometer with Depolarization	CAS-DPOL	No	Yes
Particle Habit Imaging and Polar Scattering Probe	PHIPS-HALO	No	Yes
Compact Time of Flight Aerosol Mass Spectrometer	C-ToF-AMS	No	Yes
Aerosol MEasuremenT SYSTem	AMESTYST	No	Yes
SiNgle-ParticleSOOtPhotometer System	SNOOPY	No	Yes
HALO Aerosol Submicrometer Inlet	HASI	No	Yes
Cloud Condensation Nucleus Counter	CCNC	No	Yes
Photo-Acoustic Spectrometer	PAS	No	Yes
Single Particle Soot Photometer	SP-2	No	Yes
Fast Ice Nucleus Chamber	FINCH	No	Yes
CO, O3	AMTEX	No	Yes
SO2, HNO3, PFC	PAN-MS	No	Yes
NOy, NO	IPA-NOy	No	Yes
Mini Differential Optical Absorption Spectroscopy	miniDOAS	No	Yes
Spectral Modular Airborne Radiation Measurement System	SMART	No	Yes
Imaging Spectrometer Package Eagle/Hawk		No	Yes
Hygrometer for Atmospheric Investigations	HAI	No	Yes

Table S13

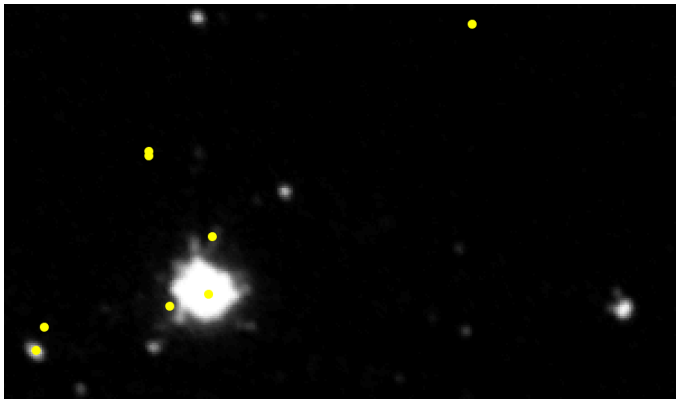

Figure S1

a. IOP1 G1 FlightTrajectories 250 m to 750 m

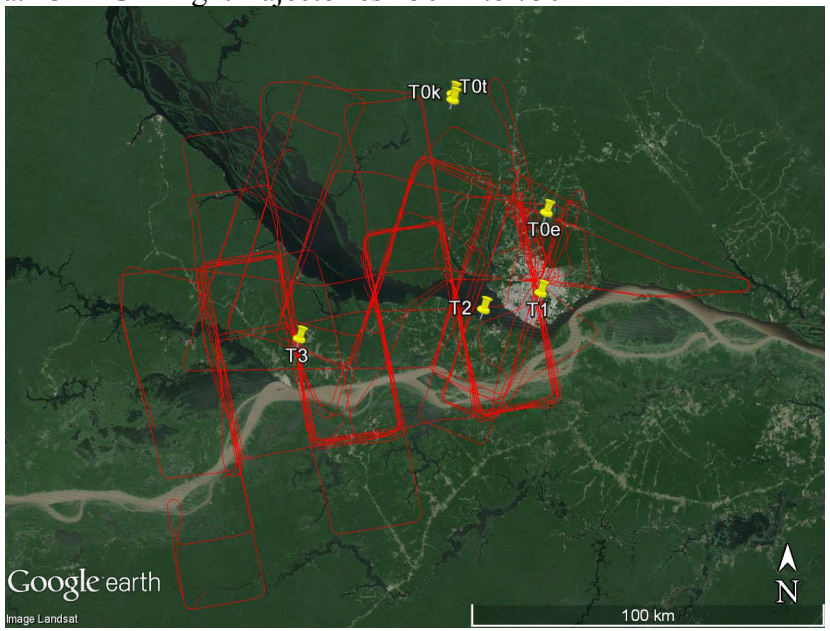

c. IOP1 G1 FlightTrajectories 1250 m to 1750 m

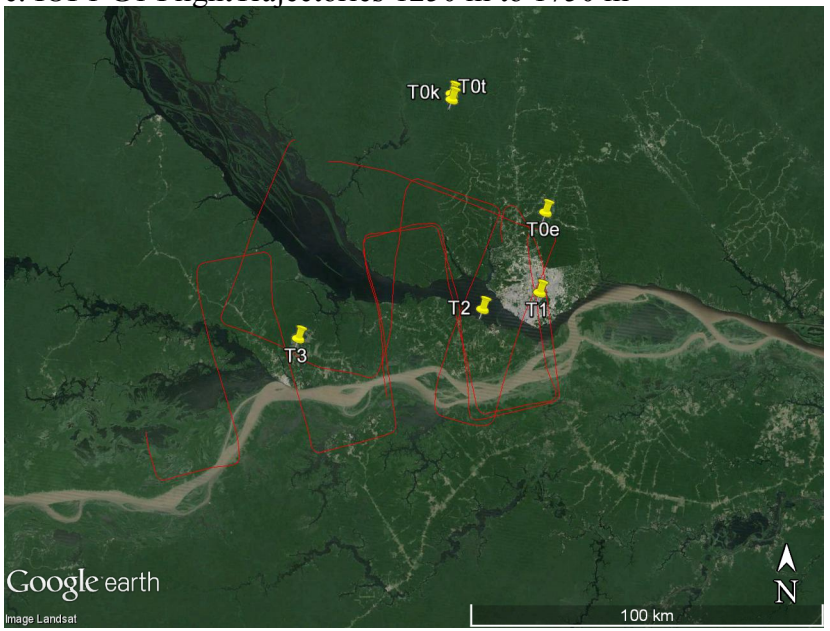

b. IOP1 G1 FlightTrajectories 750 m to 1250 m

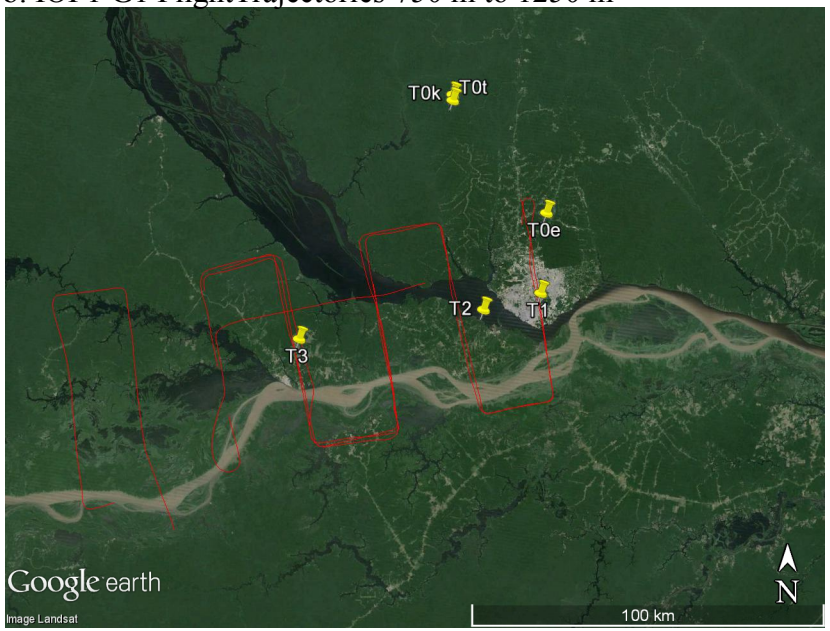

d. IOP1 G1 FlightTrajectories above 1750 m

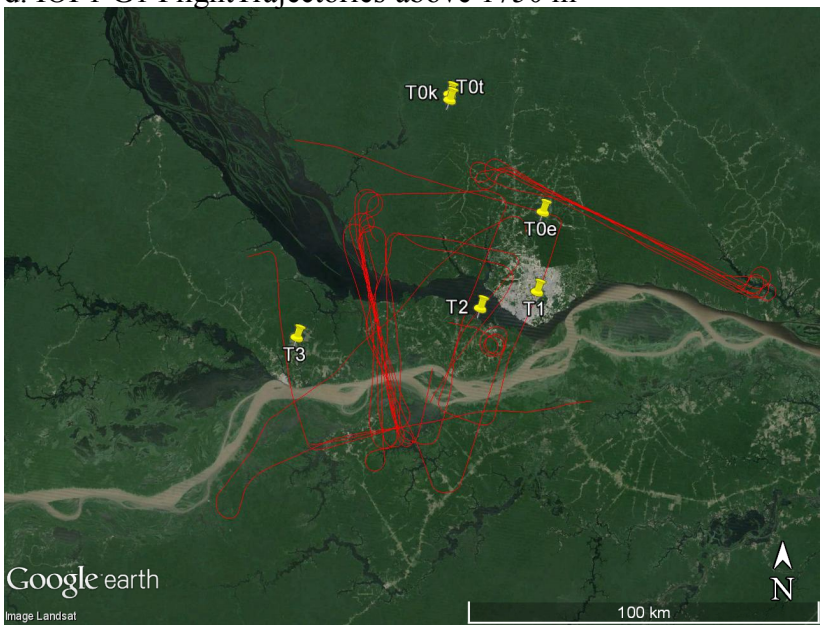

Figure S2

a. IOP2 G1 FlightTrajectories 250 m to 900 m

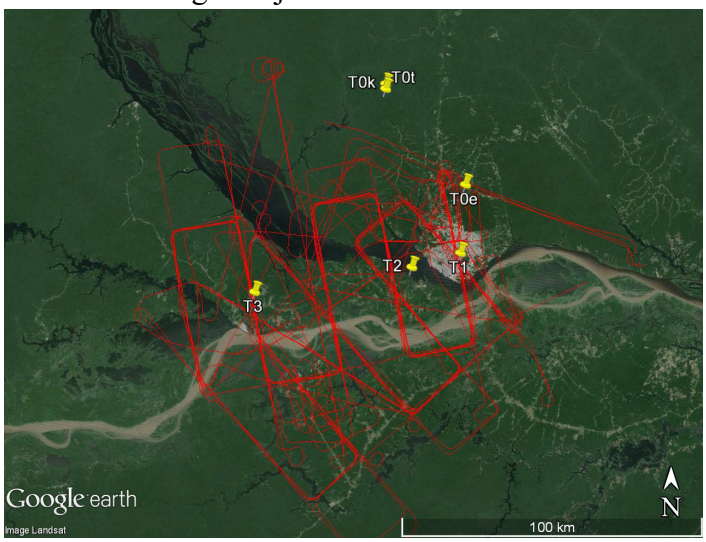

b. IOP2 G1 FlightTrajectories 1000 m to 2000 m

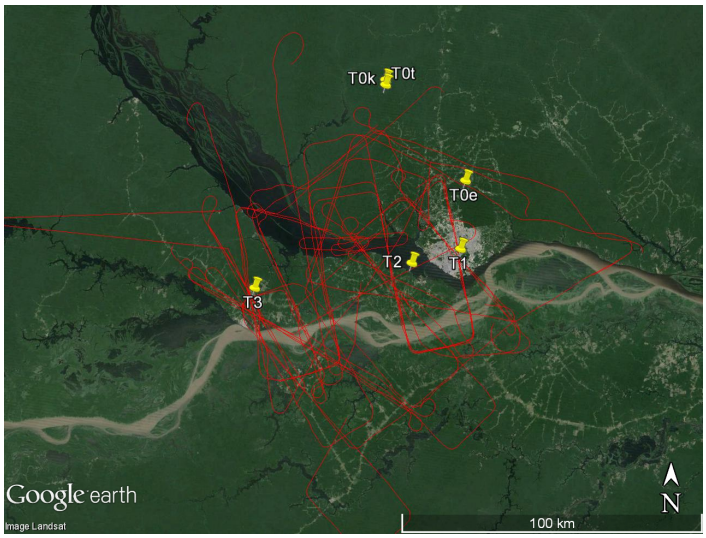

c. IOP2 G1 FlightTrajectories above 2000 m

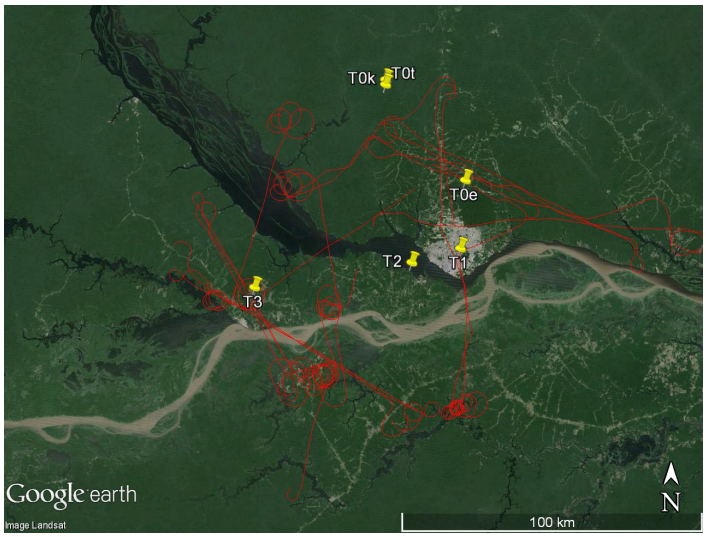

Figure S3

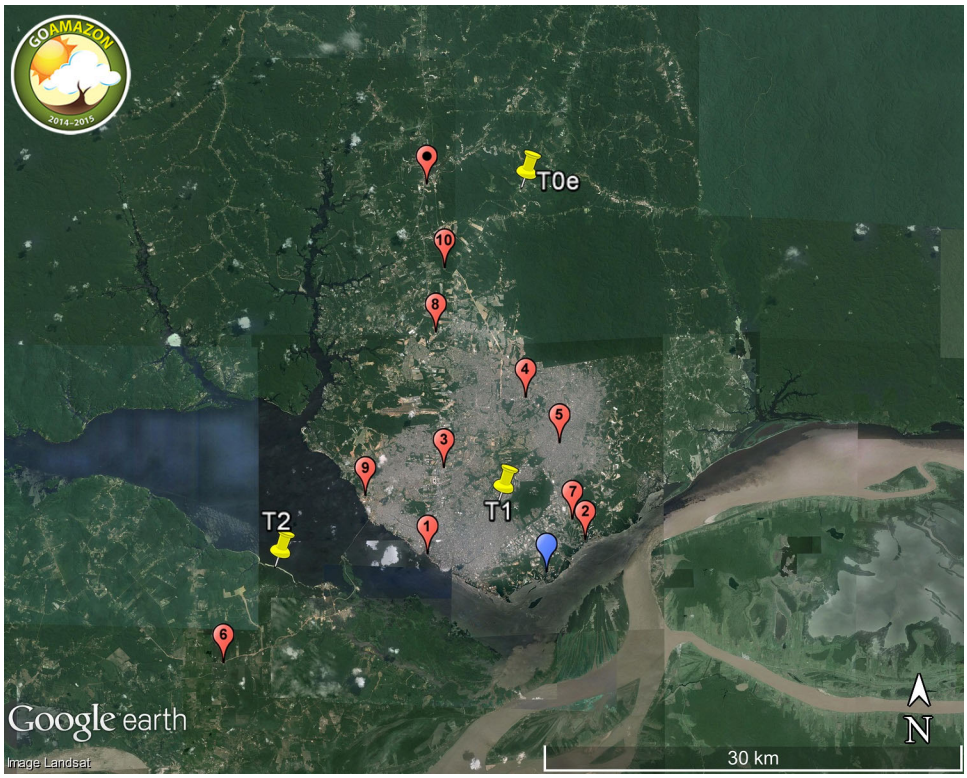
GOAMAZON
2014–2015
T0e
T1
T2
1
2
3
4
5
6
7
8
9
10
Google earth
Image Landsat
30 km
N

Figure S4

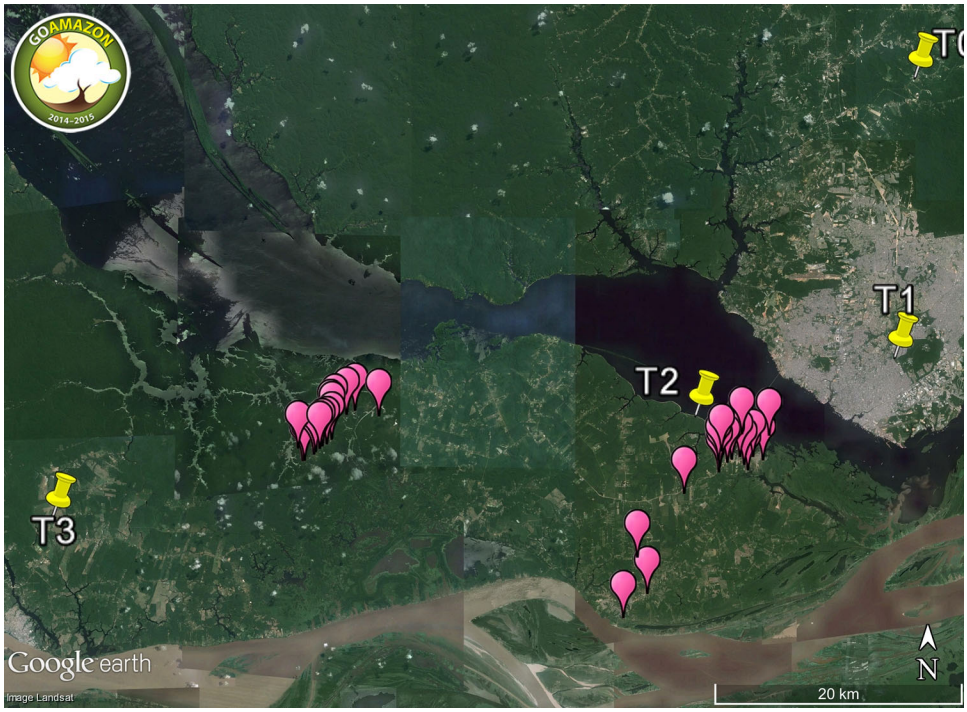
GOAMAZON
2014–2015
T0
T1
T2
T3
Google earth
Image Landsat
N
20 km

Figure S5

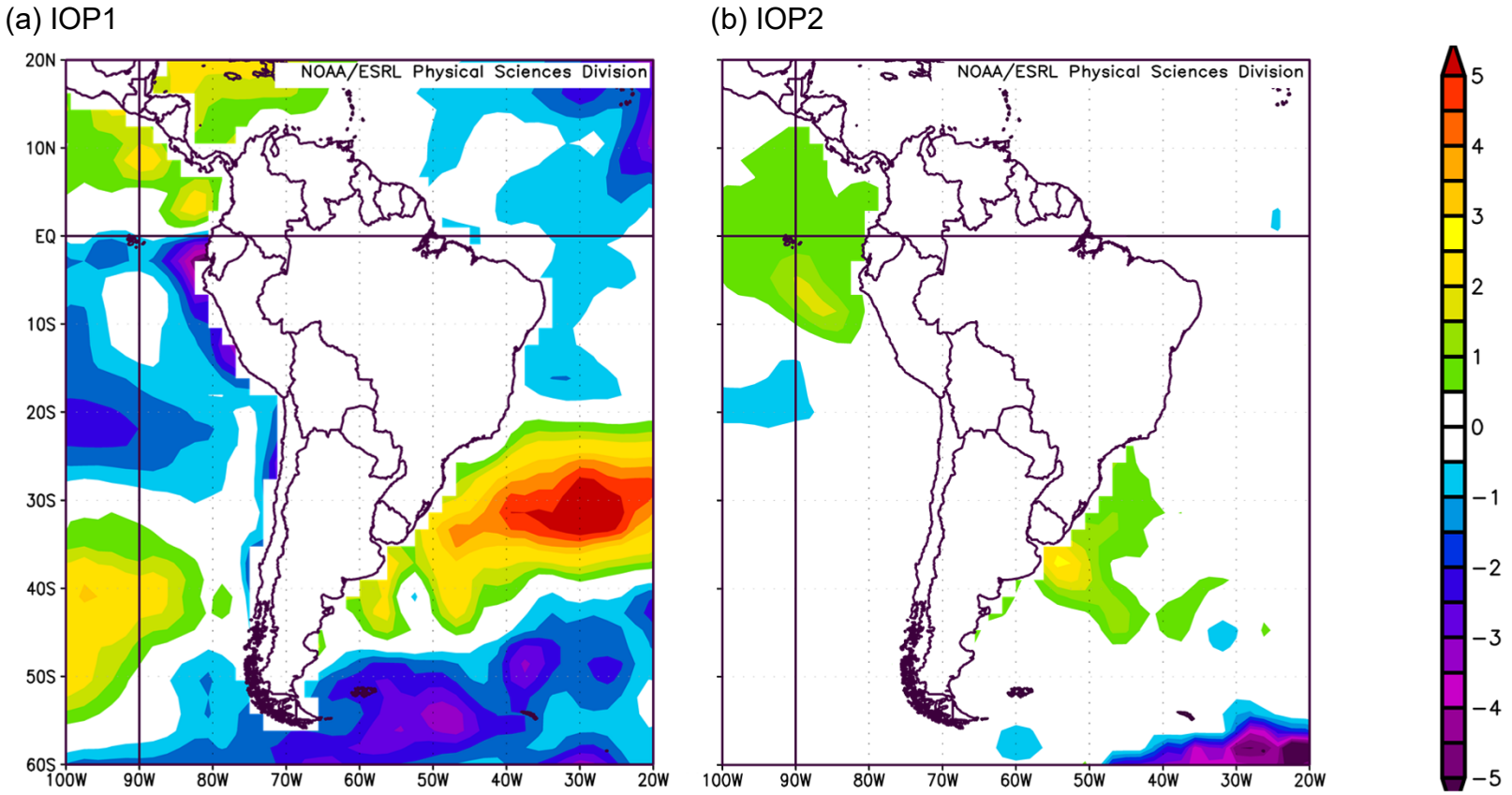
(a) IOP1
(b) IOP2
NOAA/ESRL Physical Sciences Division
NOAA/ESRL Physical Sciences Division
20N
10N
EQ
10S
20S
30S
40S
50S
60S
100W
90W
80W
70W
60W
50W
40W
30W
20W
5
4
3
2
1
0
−1
−2
−3
−4
−5

Figure S6

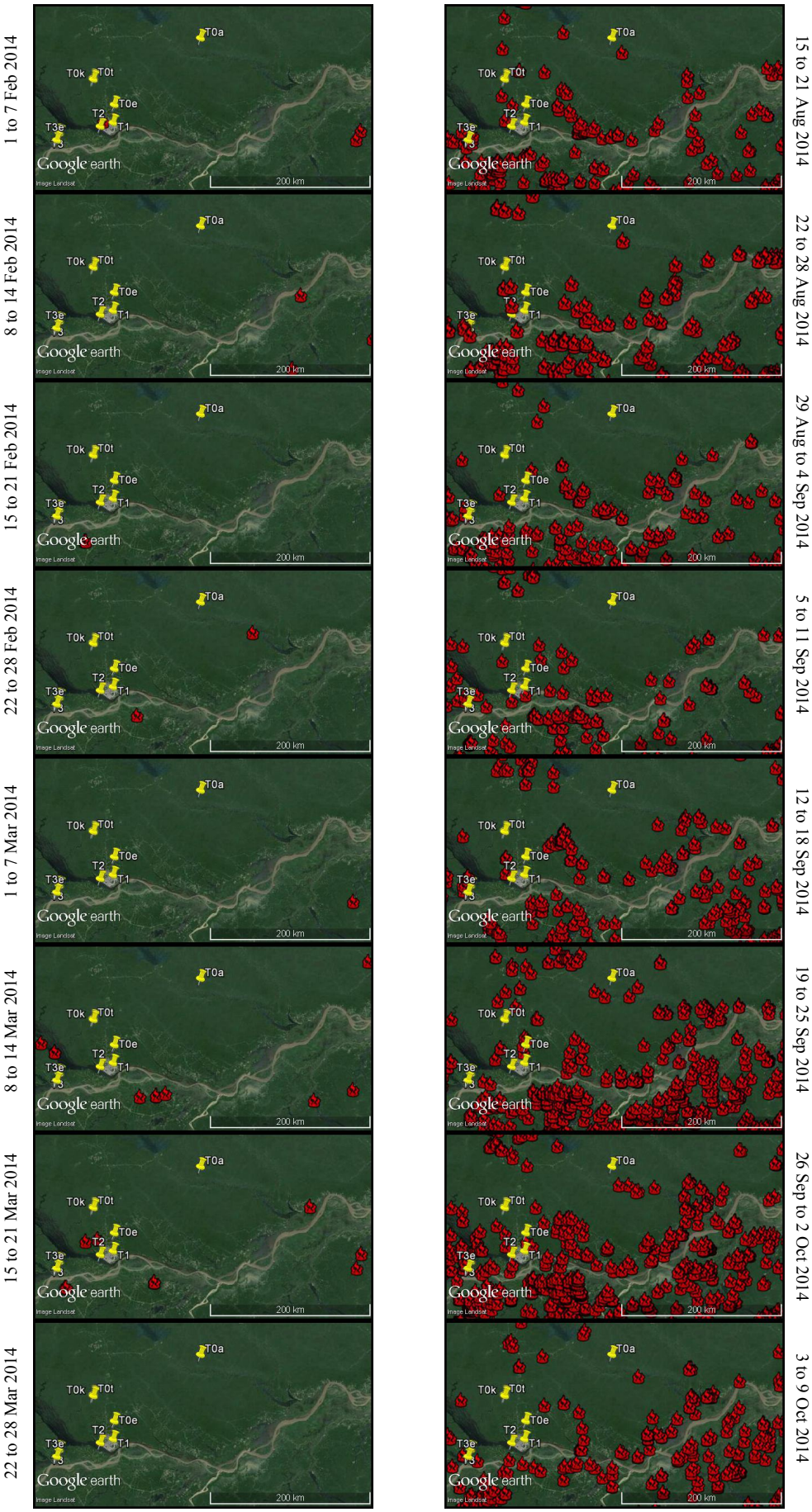
1 to 7 Feb 2014
8 to 14 Feb 2014
15 to 21 Feb 2014
22 to 28 Feb 2014
1 to 7 Mar 2014
8 to 14 Mar 2014
15 to 21 Mar 2014
22 to 28 Mar 2014
15 to 21 Aug 2014
22 to 28 Aug 2014
29 Aug to 4 Sep 2014
5 to 11 Sep 2014
12 to 18 Sep 2014
19 to 25 Sep 2014
26 Sep to 2 Oct 2014
3 to 9 Oct 2014
T0a
T0k
T0t
T0e
T2
T3e
T1
T3
Google earth
200 km

Figure S7

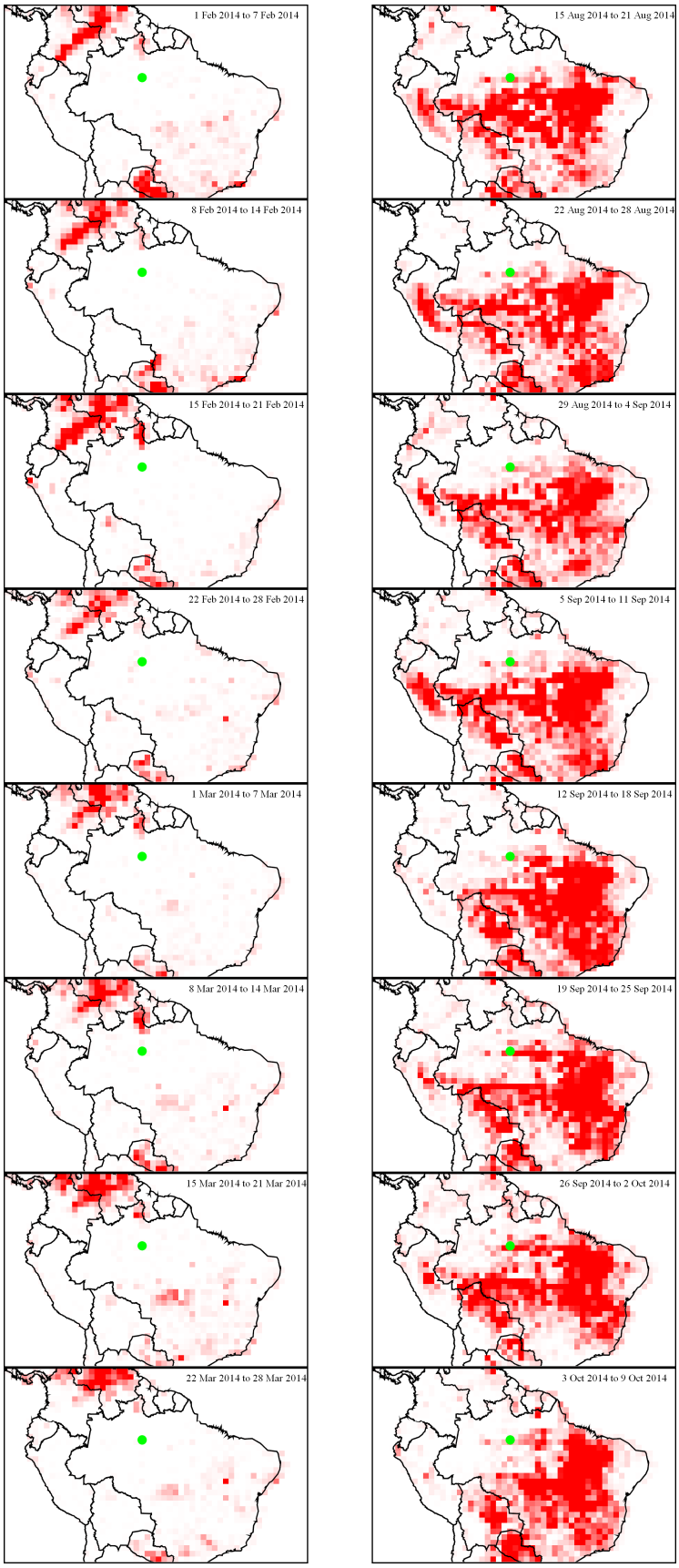
1 Feb 2014 to 7 Feb 2014
8 Feb 2014 to 14 Feb 2014
15 Feb 2014 to 21 Feb 2014
22 Feb 2014 to 28 Feb 2014
1 Mar 2014 to 7 Mar 2014
8 Mar 2014 to 14 Mar 2014
15 Mar 2014 to 21 Mar 2014
22 Mar 2014 to 28 Mar 2014
15 Aug 2014 to 21 Aug 2014
22 Aug 2014 to 28 Aug 2014
29 Aug 2014 to 4 Sep 2014
5 Sep 2014 to 11 Sep 2014
12 Sep 2014 to 18 Sep 2014
19 Sep 2014 to 25 Sep 2014
26 Sep 2014 to 2 Oct 2014
3 Oct 2014 to 9 Oct 2014

Figure S8

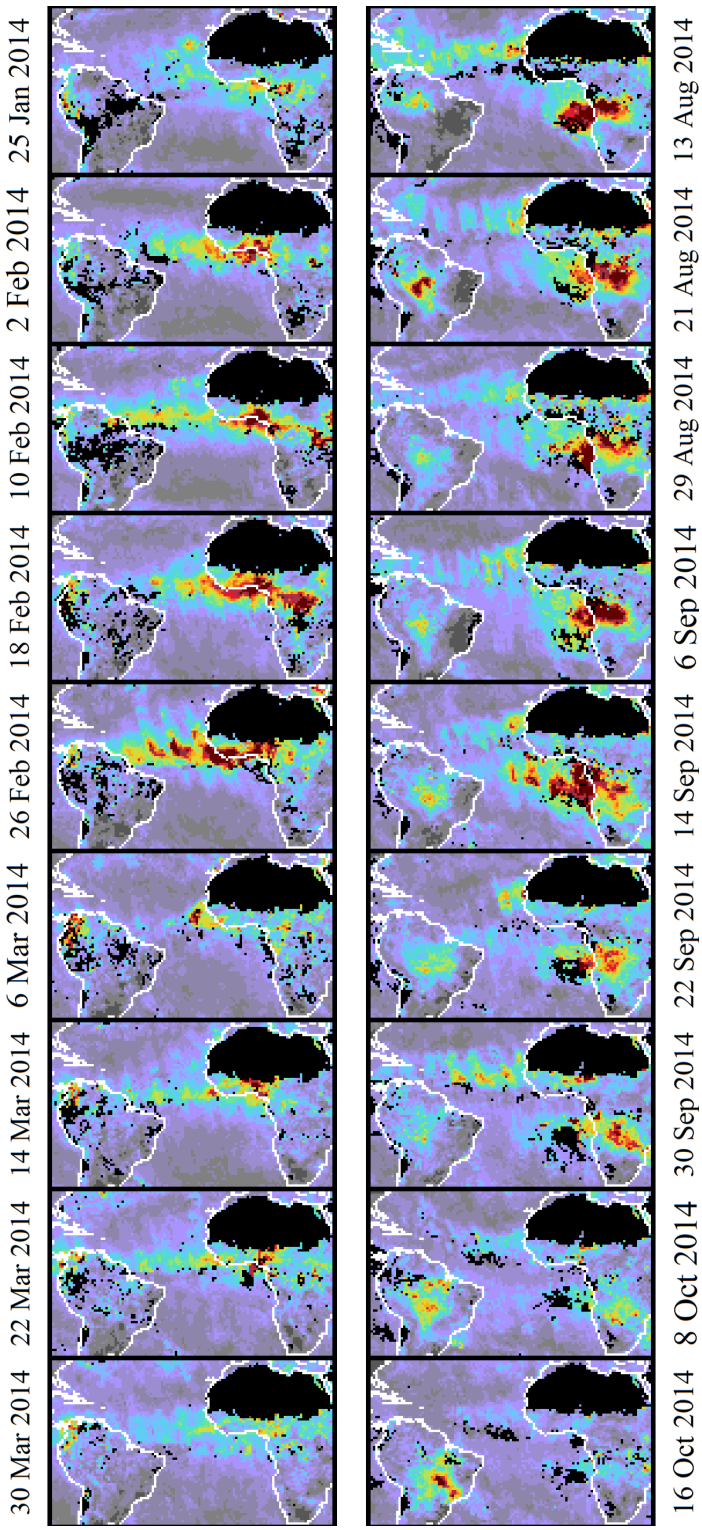
30 Mar 2014
22 Mar 2014
14 Mar 2014
6 Mar 2014
26 Feb 2014
18 Feb 2014
10 Feb 2014
2 Feb 2014
25 Jan 2014
16 Oct 2014
8 Oct 2014
30 Sep 2014
22 Sep 2014
14 Sep 2014
6 Sep 2014
29 Aug 2014
21 Aug 2014
13 Aug 2014

Figure S9